ACS APPLIED MATERIALS & INTERFACES

Open Access
This article is licensed under CC-BY-NC-ND 4.0

www.acsami.org
Research Article

Nanohydroxyapatite Coating Attenuates Fibrotic and Immune Responses to Promote Keratoprosthesis Biointegration in Advanced Ocular Surface Disorders

Arun J. Thirunavukarasu, Fernando Morales-Wong, Nuur Shahinda Humaira binte Halim, Evelina Han, Siew Kwan Koh, Lei Zhou, Viridiana Kocaba, Subramanian Venkatraman, Jodhbir S. Mehta,* and Andri K. Riau*

Cite This: *ACS Appl. Mater. Interfaces* 2024, 16, 25892−25908

Read Online

ACCESS | Metrics & More | Article Recommendations | Supporting Information

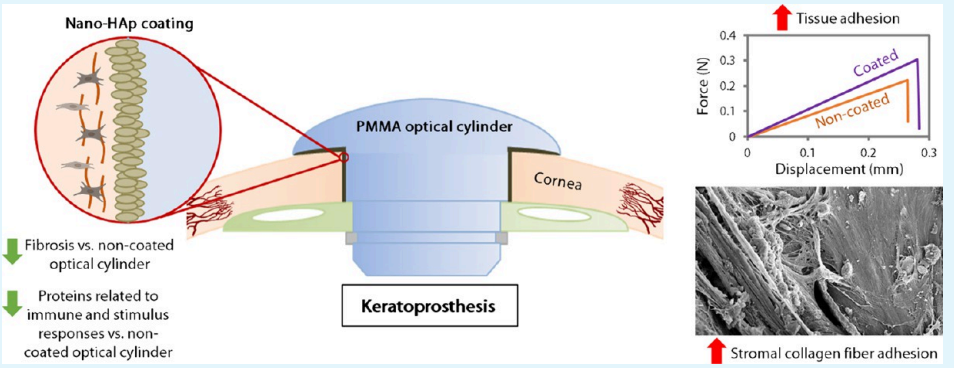

ABSTRACT: Keratoprosthesis (KPro) implantation is frequently the only recourse for patients with severe corneal disease. However, problems arise due to inadequate biointegration of the KPro, particularly the PMMA optical cylinder, such as tissue detachment, tissue melting, or eye-threatening infection in the interface. Here, using the AuroKPro as a model prosthesis, a surface functionalization approach—coating the optical cylinder with nanohydroxyapatite (nHAp)—was trialed in rabbit eyes with and without a proceeding chemical injury. In chemically injured eyes, which simulated total limbal epithelial stem cell deficiency, clear benefits were conferred by the coating. The total modified Hackett−McDonald score and area of tissue apposition differences 12 weeks after implantation were 5.0 and 22.5%, respectively. Mechanical push-in tests revealed that 31.8% greater work was required to detach the tissues. These differences were less marked in uninjured eyes, which showed total score and tissue apposition differences of 2.5 and 11.5%, respectively, and a work difference of 23.5%. The improved biointegration could be contributed by the attenuated expression of fibronectin (p = 0.036), collagen 3A1 (p = 0.033), and α-smooth muscle actin (p = 0.045)—proteins typically upregulated during nonadherent fibrous capsule envelopment of bioinert material—adjacent to the optical cylinders. The coating also appeared to induce a less immunogenic milieu in the ocular surface tissue, evidenced by the markedly lower expression of tear proteins associated with immune and stimulus responses. Collectively, the level of these tear proteins in eyes with coated prostheses was 1.1 ± 13.0% of naïve eyes: substantially lower than with noncoated KPros (246.5 ± 79.3% of naïve, p = 0.038). Together, our results indicated that nHAp coating may reduce the risk of prosthesis failure in severely injured eyes, which are representative of the cohort of KPro patients.

KEYWORDS: *cornea, biointegration, surface modification, hydroxyapatite, keratoprosthesis, immune response*

1. INTRODUCTION

For millions of patients around the world affected by corneal blindness, corneal transplant (keratoplasty) is the only means by which their vision can be restored. However, strict storage requirements for corneal allograft tissue contribute to a severe shortage, depriving many patients from the essential treatment required to restore their vision.[1] Numerous strategies to ameliorate this problem have been explored, ranging from extending the shelf life of donor tissue to designing synthetic alternatives to human corneal tissue for transplantation.[2−5] Despite these innovations, where patients exhibit severe ocular

Received: March 12, 2024
Revised: April 17, 2024
Accepted: April 18, 2024
Published: May 13, 2024

ACS Publications
© 2024 The Authors. Published by American Chemical Society

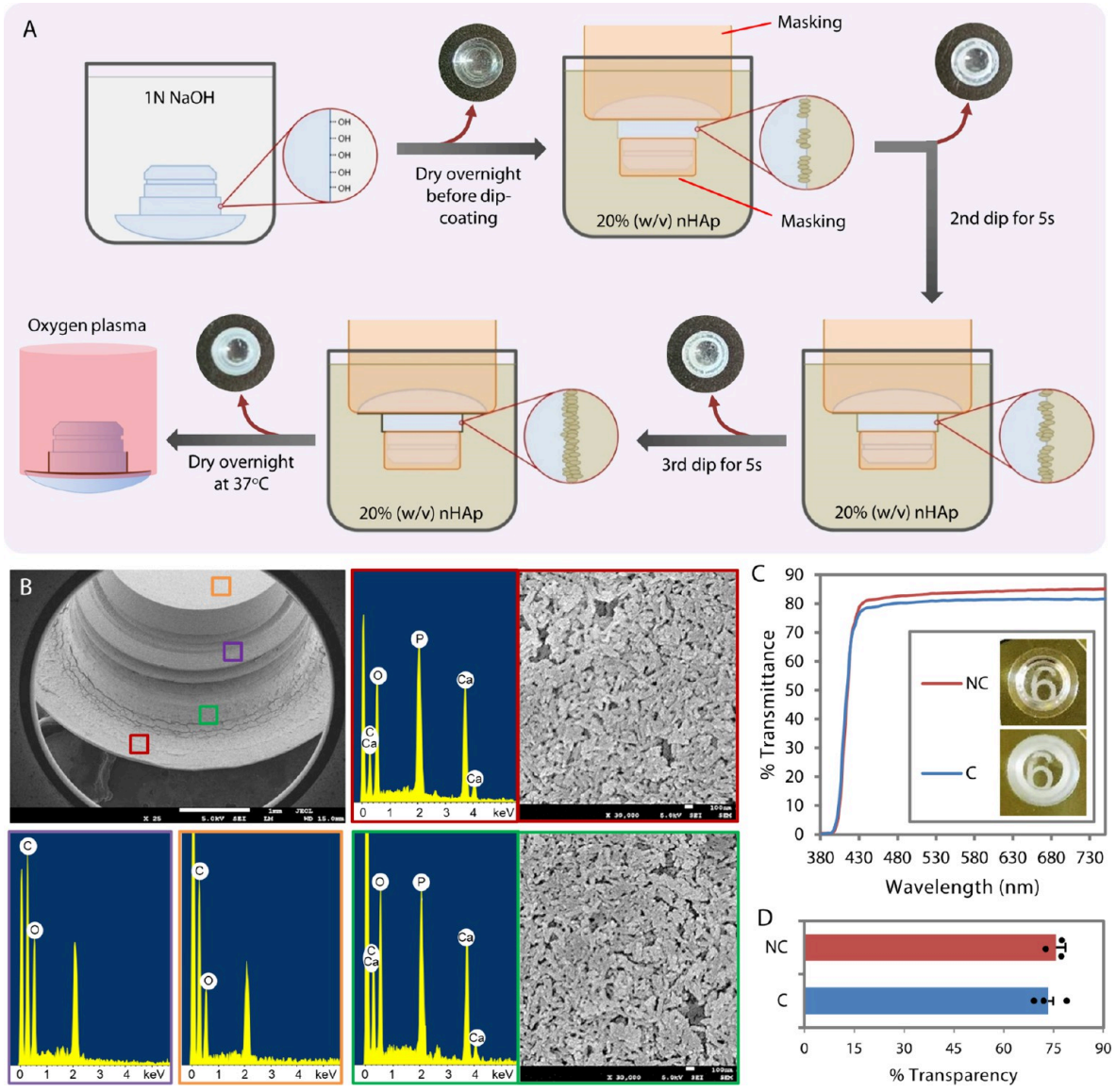

Figure 1. Basic characterization of nanohydroxyapatite (nHAp) coating outcome on the PMMA optical cylinder of AuroKPro. (A) The PMMA optical cylinder surface was primed with NaOH to prepare it for the coating process. After masking with silicone, followed by three dips for 5 s each in the nHAp-containing dip-coating solution, a thin nHAp layer formed on the PMMA surface. The contaminants and excess PMMA were then removed with oxygen plasma treatment. (B) Scanning electron microscopy (SEM) and energy-dispersive X-ray (EDX) revealed the presence of rod-shaped nHAp (also indicated by the calcium or Ca and phosphorus or P elements) only on the desired regions of the optical cylinder, namely, the posterior side of the optic dome (highlighted in red) and the wall of the first segment of the cylinder stem (highlighted in green). The rest of the optical cylinder (orange and purple highlighted regions) was devoid of nHAp due to the masking applied during the dip-coating process. Scale bars = 1 mm in low-magnification image and 100 nm in high-magnification images. (C) The nHAp-coated PMMA optical cylinder did not compromise the light transmittance across visible-light wavelengths. (D) Quantitatively, the transmittance level was not significantly different from the noncoated optical cylinder (p = 0.512). Data are presented as mean ± SE (n = 3 in each group). NC = noncoated. C = coated.

surface disease or a history of multiple graft failures, conventional keratoplasty procedures may be unlikely to succeed.[6] In these cases, a keratoprosthesis (KPro)—a prosthetic cornea, such as MICOF KPro, Boston KPro, AuroKPro, and osteo-odonto KPro—may be the only recourse for management.[7,8]

The most widely used KPro—the Boston KPro—has a core-skirt design with transparent optical core composed of bioinert poly(methyl methacrylate) (PMMA) and skirt composed of biological material (donor corneal tissue).[9] The AuroKPro (Aurolab, Madurai, India) features a similar design with comparable functional outcomes, and its affordability confers better accessibility for clinical use, particularly in resource-constrained settings.[10] Polymers such as PMMA, poly(lactic-*co*-glycolic acid), and polyethylene are commonly used as substrates or scaffolds across many surgical specialties. The inert and hydrophobic properties of these materials, however, induce fibrous tissue envelopment and do not elicit any biological function within adjacent tissue, which is necessary for biointegration.[11,12] In KPros, poor biointegration can result in epithelial ingrowth, graft separation or cavitation, corneal melting, aqueous humor leakage, and intraocular infection, leading to implant failure and extrusion requiring further surgery and potentially compromising patient outcomes.[13−16] Despite these risks, KPro is the only management option where conventional keratoplasty has a high risk of failure, such as in

https://doi.org/10.1021/acsami.4c04077
ACS Appl. Mater. Interfaces 2024, 16, 25892−25908

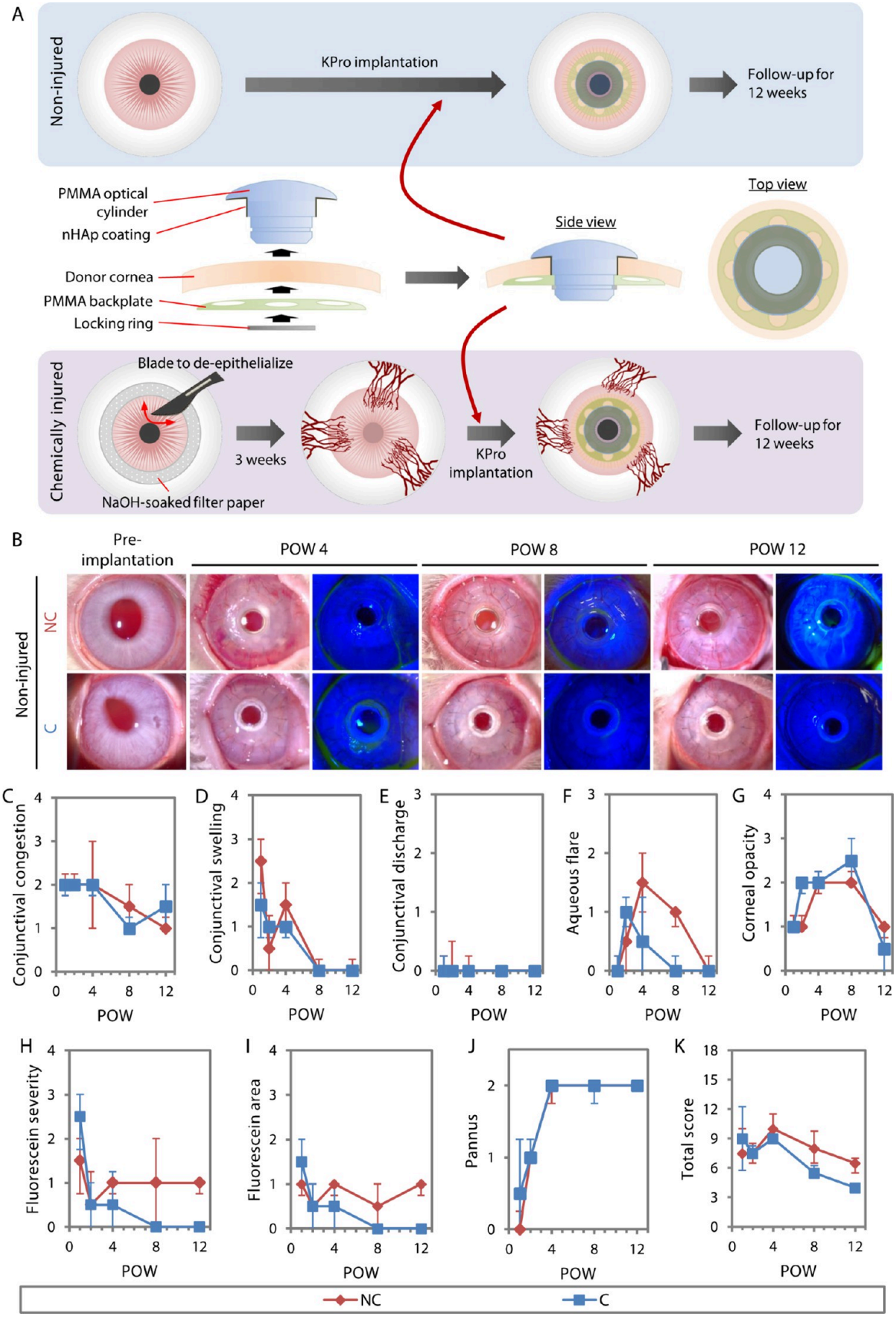

Figure 2. Clinical outcomes of AuroKPro implantation in noninjured rabbit corneas. (A) After the KPros were assembled, they were implanted in two rabbit experimental models: noninjured model (naive cornea) and chemically injured model (alkali burn cornea). (B) In the noninjured model, slit-lamp images showed that nHAp-coated KPro implantation had a rather similar clinical outcome as the noncoated KPro, except for the presence of a faint fluorescein track under the dome of the noncoated KPro optical cylinder at weeks 8 and 12. Over 12 weeks, both eyes implanted with noncoated

https://doi.org/10.1021/acsami.4c04077
ACS Appl. Mater. Interfaces 2024, 16, 25892−25908

Figure 2. continued

and coated prostheses demonstrated improving conjunctival congestion (C), conjunctival swelling (D), conjunctival discharge (E), aqueous flare (F), and corneal opacity (G). The fluorescein staining severity (H) and fluorescein staining area (I) were greater in the eyes with coated KPros at week 1 but improved over time. In contrast, the eyes with noncoated KPros had persistent fluorescein staining at all time points. Although the severity of neovascularization reached the plateau at week 4 and did not improve over time (J), the total modified Hackett−McDonald score indicated an overall improvement in corneal and conjunctival conditions in both groups (K). Although not statistically significant, at week 12, the coated KPros produced a 2.5 median better total score than the noncoated KPros. The clinical grading outcomes ($n = 4$ in each group) are presented in the median (data points) and quartile 1 and quartile 3 (lower and upper limits of the error bars). NC = noncoated. C = coated. POW = postoperative week.

diseases of the cornea with extensive limbal stem cell deficiency and vascularization, as seen following chemical burns.[10,17,18]

Surface modification approaches, where microscale or nanoscale regions of biochemically and topographically optimized material are produced, without changing the properties of the implant, have proven promising in the field of biomedical engineering. A common surface modification approach is hydroxyapatite (HAp) coating, which has been applied to various dental, ophthalmological, and orthopedic implants.[19−23] The HAp coating acts as a bioactive surface for the bioinert implants and functions to induce tissue responses, which are essential for biointegration, such as mitigation of inflammation and reduction of fibrosis in the host tissues.[22,24,25] However, while applications in load-bearing implants are well established in the clinic, most other examples have not progressed from bench to bedside.[26,27]

Surface engineering of existing KPro designs is an attractive solution because of the reduced requirement to validate new primary components before clinical trials can be conducted and implants accepted for clinical use.[28] A wide variety of coating techniques exist for applying HAp to a surface, many of which involve significant heat, which would compromise the physical and biochemical characteristics of a KPro.[27,29,30] Our previous work established and optimized a dip-coating technique to immobilize nano-HAp (nHAp) on acrylic sheets and rods.[25,31] Here, we applied the technique to clinical-grade AuroKPros and evaluated the preclinical outcomes and potential biomechanical advantages in a rabbit model of corneal surgery with and without prior chemical burn to explore the clinical potential of this affordable surface modification approach. In addition, we also studied tissue fibrotic responses and temporal tear proteomics to uncover the potential mechanism of action by which the nHAp coating supports biointegration.

2. RESULTS

2.1. Immobilization of Nanohydroxyapatite on the PMMA Optical Cylinder. We attempted to coat the PMMA optical cylinder of AuroKPro by following our previous method, where we showed that nHAp was uniformly immobilized on the periphery of a 3 mm-diameter PMMA cylinder by dipping the cylinder in the dip-coating solution thrice 5 s each.[25] However, this method resulted in a mm-thick nHAp coating, which was not adherent to the surface of the PMMA optical cylinder. This was due to a lack of "softening" of the PMMA surface during dip-coating, which caused the nHAp coating to delaminate due to weak binding to the PMMA. Instead, we opted to prime the surface by treating it with 1 N NaOH (to reduce the hydrophobicity of the PMMA), followed by dipping in chloroform and 2.5% (w/v) PMMA in chloroform (Figure 1A). After three 5 s dips in the dip-coating solution, a thin nHAp layer covered the PMMA surface—the posterior side of the optic dome and wall of the first segment of the optical cylinder stem—which would be in direct contact with the donor corneal tissue (Figure 1A).

High-magnification scanning electron microscopy (SEM) images of the aforementioned two regions (highlighted in red and green, respectively) revealed the presence of rod-shaped nHAp, consistent with the shape of the nHAp that was mixed in the dip-coating solution (Figure 1B). The energy-dispersive X-ray (EDX) confirmed the appearance of calcium (Ca) and phosphorus (P) elements only in the two desired areas and not in the other regions of the optical cylinder, specifically the wall of the segment of the optic stem anterior to the groove for the locking ring (highlighted in purple) and the last segment of the stem (highlighted in orange). In the posterior two segments of the optical cylinder, a high-intensity Ca K-band at 3.7 keV and a P K-band at 2.0 keV—seen in the anterior segments covered with nHAp—were absent. The carbon (C) and oxygen (O) elements of the PMMA were discernible in all four segments, where high-intensity C K and O K bands appeared at 0.3 and 0.5 keV, respectively, on EDX. Most importantly, the dip-coating process did not significantly affect the light transmittance across the visible-light wavelength of the PMMA optical cylinder (Figure 1C). On average, the noncoated and coated optical cylinders had 75.7 ± 1.6 and 73.3 ± 2.9% transparency, respectively ($p = 0.512$) (Figure 1D).

2.2. Clinical Outcomes Following AuroKPro Implantation. Implantation of either a nHAp-coated or noncoated AuroKPro was conducted in rabbits either with or without a proceeding chemical injury (Figure 2A). The implantation in the noninjured cornea served as a baseline and safety assessment of the coating *in vivo*, while implantation following induced chemical injury was done to study the performance of the coating in total limbal epithelial stem cell deficiency (LSCD).[32] In noninjured corneas, slit-lamp photographs indicated no gross difference in the clinical appearances of eyes following coated and noncoated KPro implantation (Figure 2B). Conjunctival hyperemia was more distinct in the first 4 weeks but became less severe over time in both groups. A faint fluorescein track could be seen sipping under the dome of the noncoated KPro optical cylinder at weeks eight and 12—an indication of an insecure seal between the tissue and the device. Formal grading of the clinical outcome revealed no significant differences in any scoring category and the total score between eyes implanted with coated and noncoated prostheses (Figure 2C−K and Table S1), and the only median recorded differences over 1 were as follows: 1 higher aqueous flare score at 4 and 8 weeks (Figure 2F and Table S1), 1 higher fluorescein severity score at 8 and 12 weeks (Figure 2H and Table S1), and 1 higher fluorescein area score at 12 weeks (Figure 2I and Table S1) in the eyes with noncoated KPros. Interestingly, the fluorescein staining severity and area were greater in the eyes with coated KPros at week 1 but the ocular surface defects improved over time—none of the rabbits had staining after 8 weeks. In contrast, the eyes with noncoated KPros had persistent fluorescein staining at all follow-up

https://doi.org/10.1021/acsami.4c04077
ACS Appl. Mater. Interfaces 2024, 16, 25892−25908

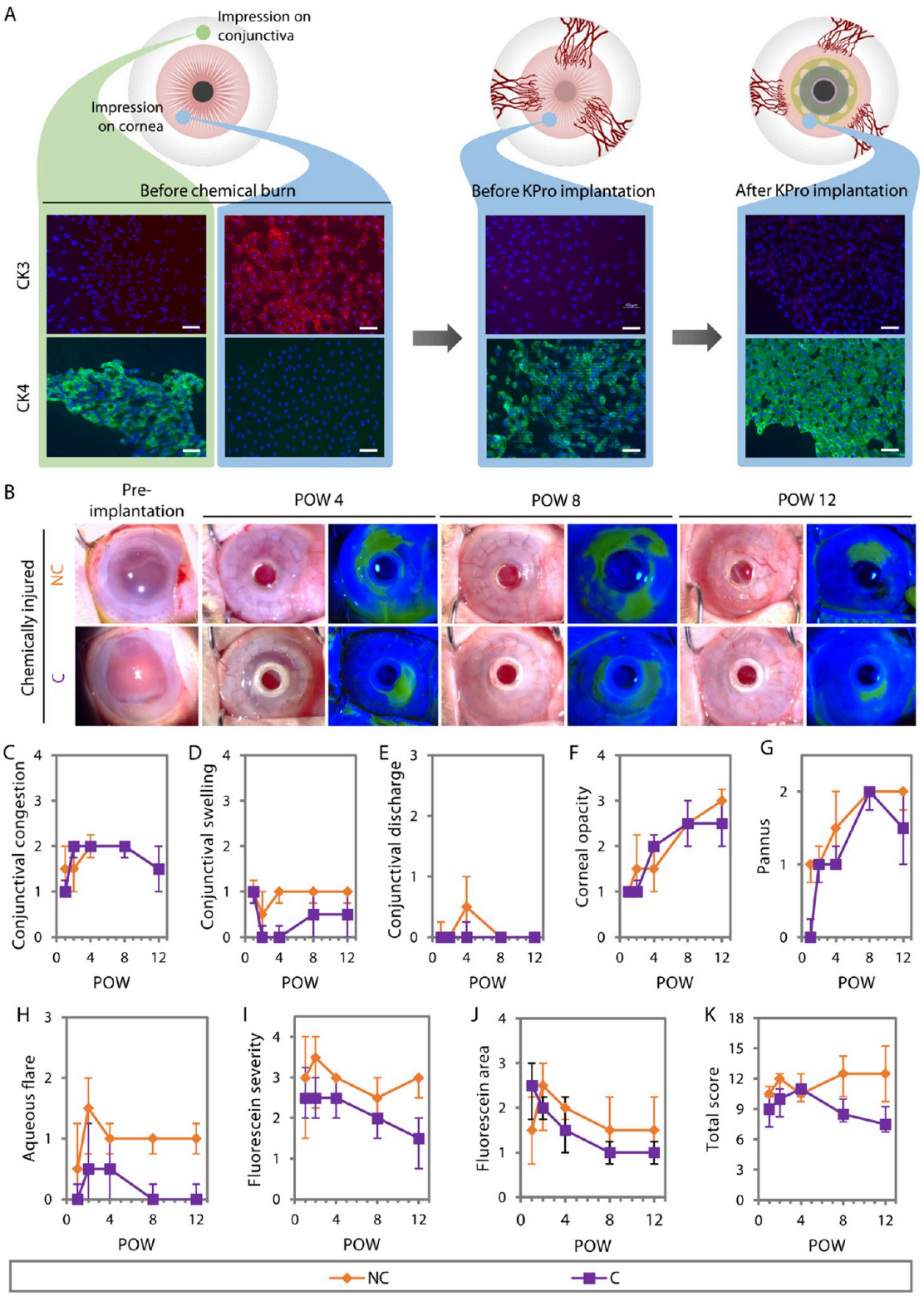

Figure 3. Clinical outcomes of AuroKPro implantation in rabbit corneas chemically injured by alkaline burns. (A) Impression cytology staining with cytokeratin (CK) 3 and CK4, representing corneal and conjunctival epithelial cell markers, respectively confirmed the occurrence of limbal epithelial stem cell deficiency, where the impression of the paracentral cornea was positive for CK4, instead of CK3. The penetration of conjunctival epithelial cells persisted after the KPro implantation. Scale bars = 50 μm. (B) Slit lamp images showed increasing corneal opacity and neovascularization over time regardless of nHAp coating presence. However, there was reduced fluorescein staining following the implantation of coated KPro relative to uncoated KPro. Based on the modified Hackett−McDonald scoring system, coated and uncoated groups exhibited similar conjunctival congestion (C), conjunctival swelling (D), conjunctival discharge (E), and corneal opacity (F) at 12 weeks. However, coated KPros were associated with less neovascularization (G), aqueous flare (H), fluorescein staining severity (I), and fluorescein staining area (J) at 12 weeks, which drove an overall improvement of the clinical score (K). The clinical grading outcomes (n = 4 in each group) are presented in the median (data points) and quartile 1 and quartile 3 (lower and upper limits of the error bars). NC = noncoated. C = coated. POW = postoperative week.

https://doi.org/10.1021/acsami.4c04077
ACS Appl. Mater. Interfaces 2024, 16, 25892−25908

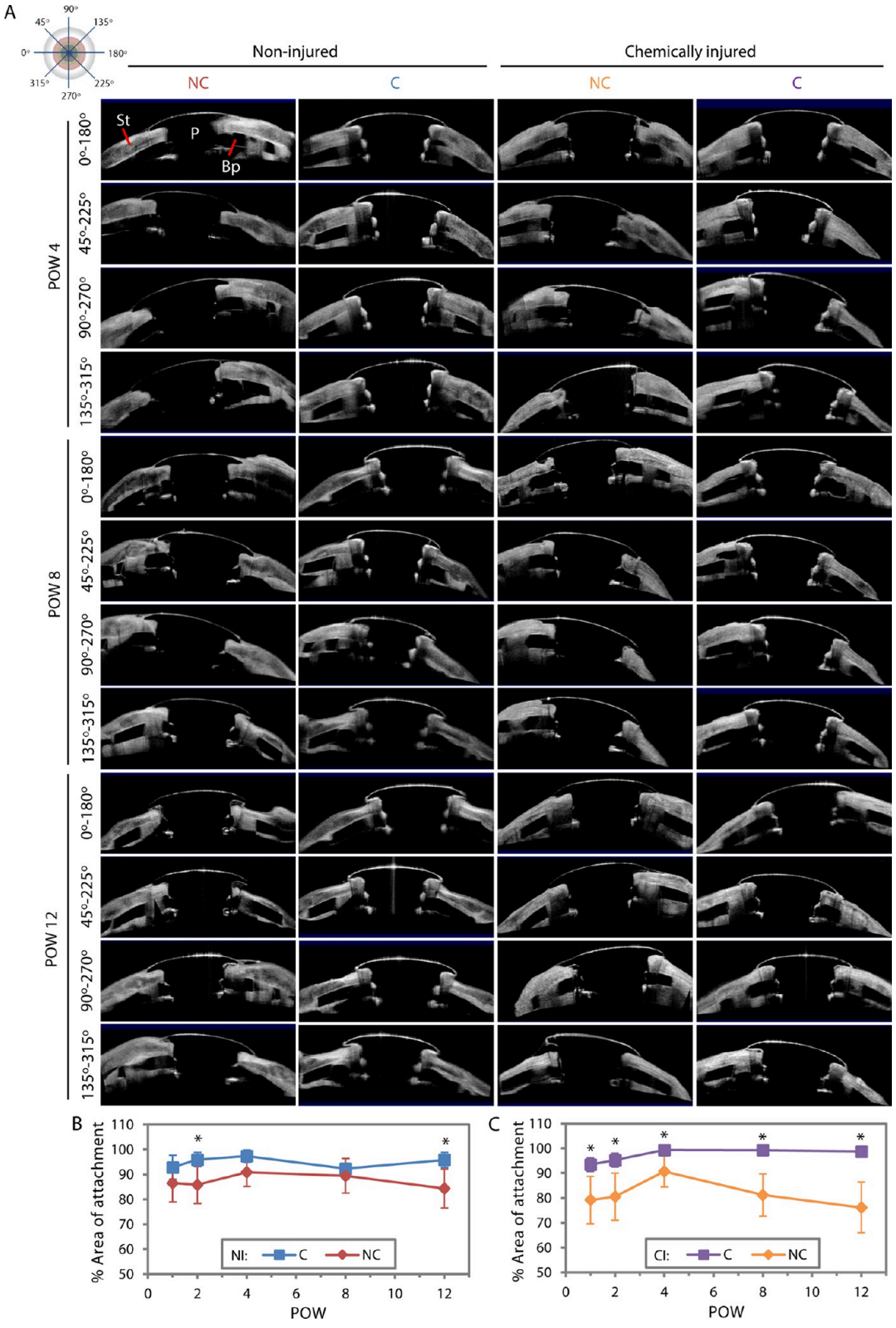

Figure 4. Corneal tissue apposition on PMMA optical cylinders following AuroKPro implantation. (A) Anterior segment-optical coherence tomography (AS-OCT) visualizations of corneal cross sections at four different meridians. On the scan, the PMMA optical cylinder (P) and backplate (Bp) appeared transparent with reflective outlines. The corneal stromal tissue (St), which appeared hyperreflective, was situated anterior to the backplate. (B) Tissue adhesion quantified as the percentage area of attachment for coated and noncoated KPros in rabbit corneas without prior chemical injury, and (C) tissue adhesion for coated and noncoated KPros in rabbit corneas with a preceding chemical burn. Tissue apposition was superior for nHAp-coated KPros in noninjured corneas at 2 and 12 weeks postoperatively, and at every postoperative time point in chemically injured corneas. Data are presented as mean ± SE (n = 4 in each group). *$p < 0.05$. NI = noninjured. CI = chemically injured. NC = noncoated. C = coated. POW = postoperative week.

https://doi.org/10.1021/acsami.4c04077
ACS Appl. Mater. Interfaces 2024, 16, 25892−25908

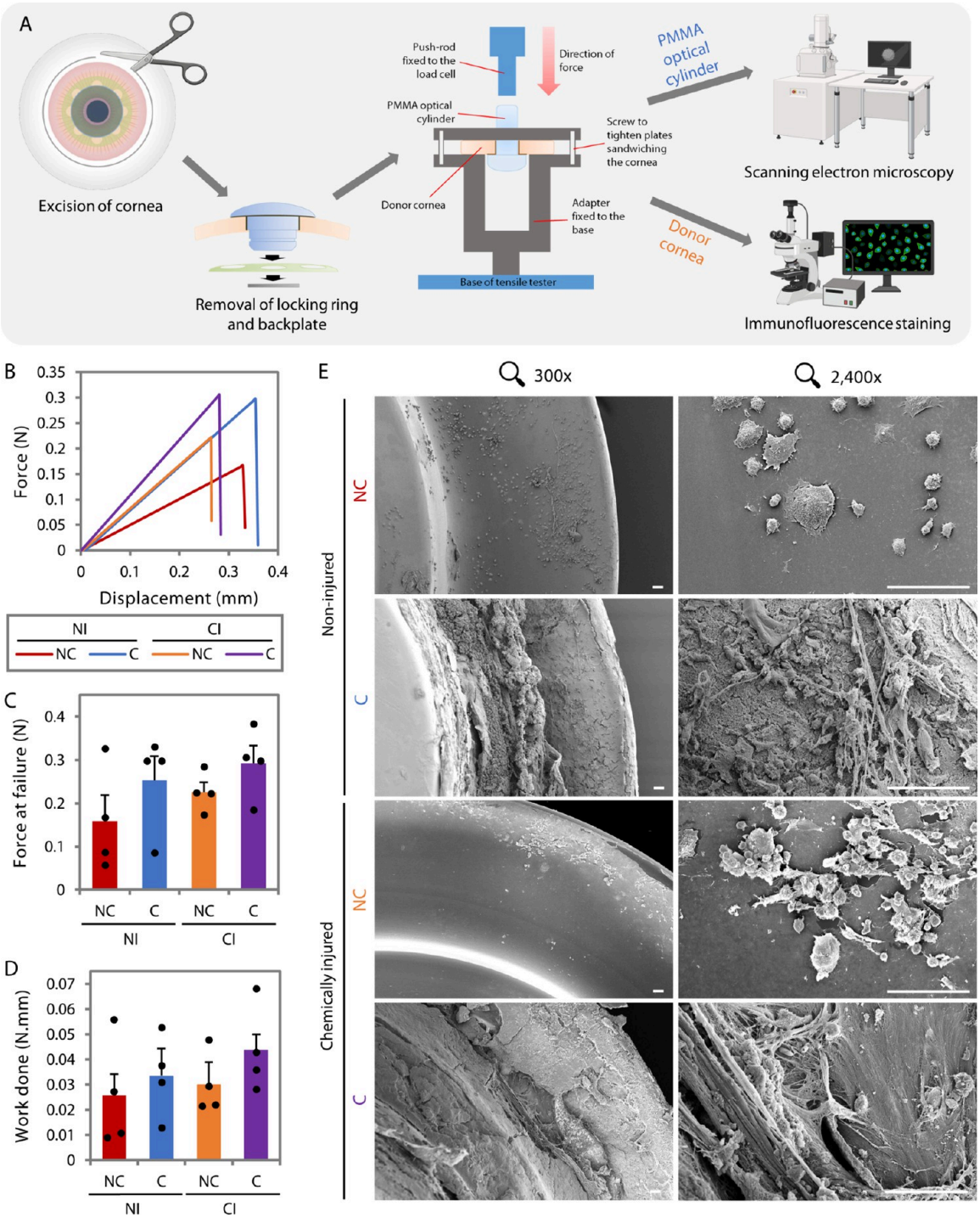

Figure 5. Corneal tissue adhesion on PMMA optical cylinders following AuroKPro implantation. (A) Excised cornea containing implanted KPro had the locking ring and backplate removed before being exposed to a mechanical push-in test to detach the optical cylinder from the surrounding cornea. Detached PMMA then underwent SEM and the cornea, immunohistochemical analysis. (B) Coated KPros required greater force to displace and detach them from the cornea than the noncoated KPros. Both KPros showed linear stress−strain curves, suggesting a similar process of tissue detachment. (C) Force at failure was greater for nHAp-coated than noncoated KPros, but differences did not reach statistical significance. (D) Similarly, greater work done in detaching coated than noncoated KPros was recorded, but differences did not arrive at statistically significant levels. (E) The SEM revealed the predominant presence of bundles of collagen fibers on the nHAp-coated optical cylinders but not on the noncoated ones. Instead, a mixture of cuboidal and cornified epithelial cells was seen on the noncoated PMMA, suggesting the epithelial ingrowth in the space between the optical cylinders and donor corneas due to poor attachment. Scale bars = 50 μm. Data are presented as mean ± SE (n = 4 in each group). NI = noninjured eyes. CI = chemically injured eyes. NC = noncoated. C = coated.

periods. Consequently, the total scores were greater than 2.5 in the eyes with noncoated prostheses at weeks 8 and 12 than those with coated implants (Figure 2K and Table S1).

In the chemical injury model, the occurrence of total LSCD, typically marked by the encroachment of conjunctival epithelial cells onto the corneal surface,[33] was confirmed when the

https://doi.org/10.1021/acsami.4c04077
ACS Appl. Mater. Interfaces 2024, 16, 25892−25908

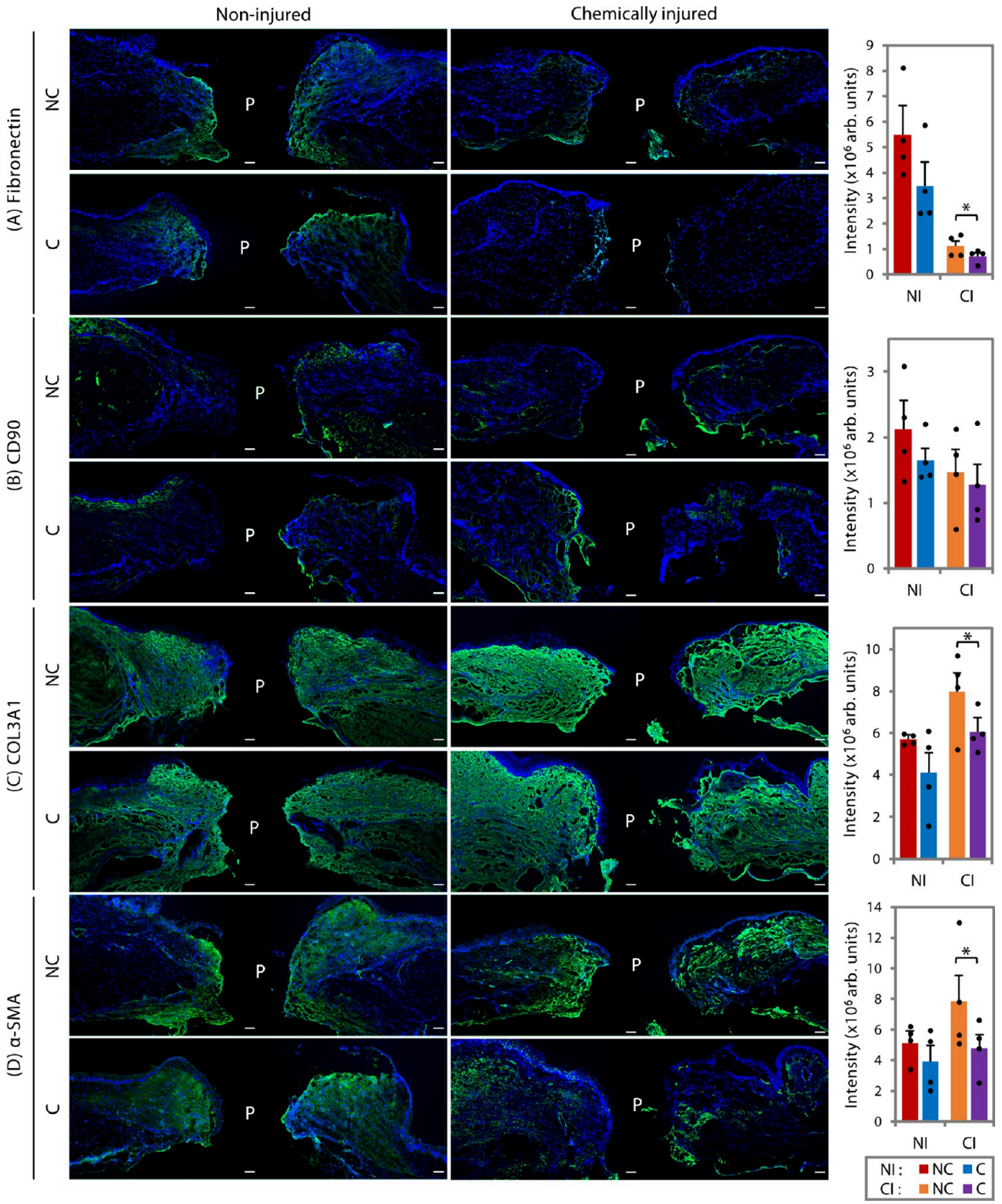

Figure 6. Corneal tissue fibrotic responses to the AuroKPro implantation. The responses were visualized and quantified with immunohistochemical analysis testing for four markers of fibrosis: fibronectin (A), CD90 (B), collagen 3A1 or COL3A1 (C), and α-smooth muscle actin or α-SMA (D). In chemically injured corneas, all markers, except CD90, were expressed in the tissue adjacent to the PMMA optical cylinders at a significantly higher level following implantation of noncoated KPros relative to nHAp-coated KPros. In noninjured situations, all fibrosis markers appeared greater with the noncoated KPros but the differences were not statistically significant. P indicates the space vacated by the PMMA optical cylinder. Scale bars = 50 μm. Data are presented as mean ± SE (n = 4 in each group). *$p < 0.05$. NI = noninjured eyes. CI = chemically injured eyes. NC = noncoated. C = coated.

impression cytology of the paracentral cornea stained positive for cytokeratin (CK) 4 (conjunctival epithelial marker as shown in the impression taken from the conjunctival surface of naïve cornea) but negative for CK3 (corneal epithelial marker) at 3

https://doi.org/10.1021/acsami.4c04077
ACS Appl. Mater. Interfaces 2024, 16, 25892−25908

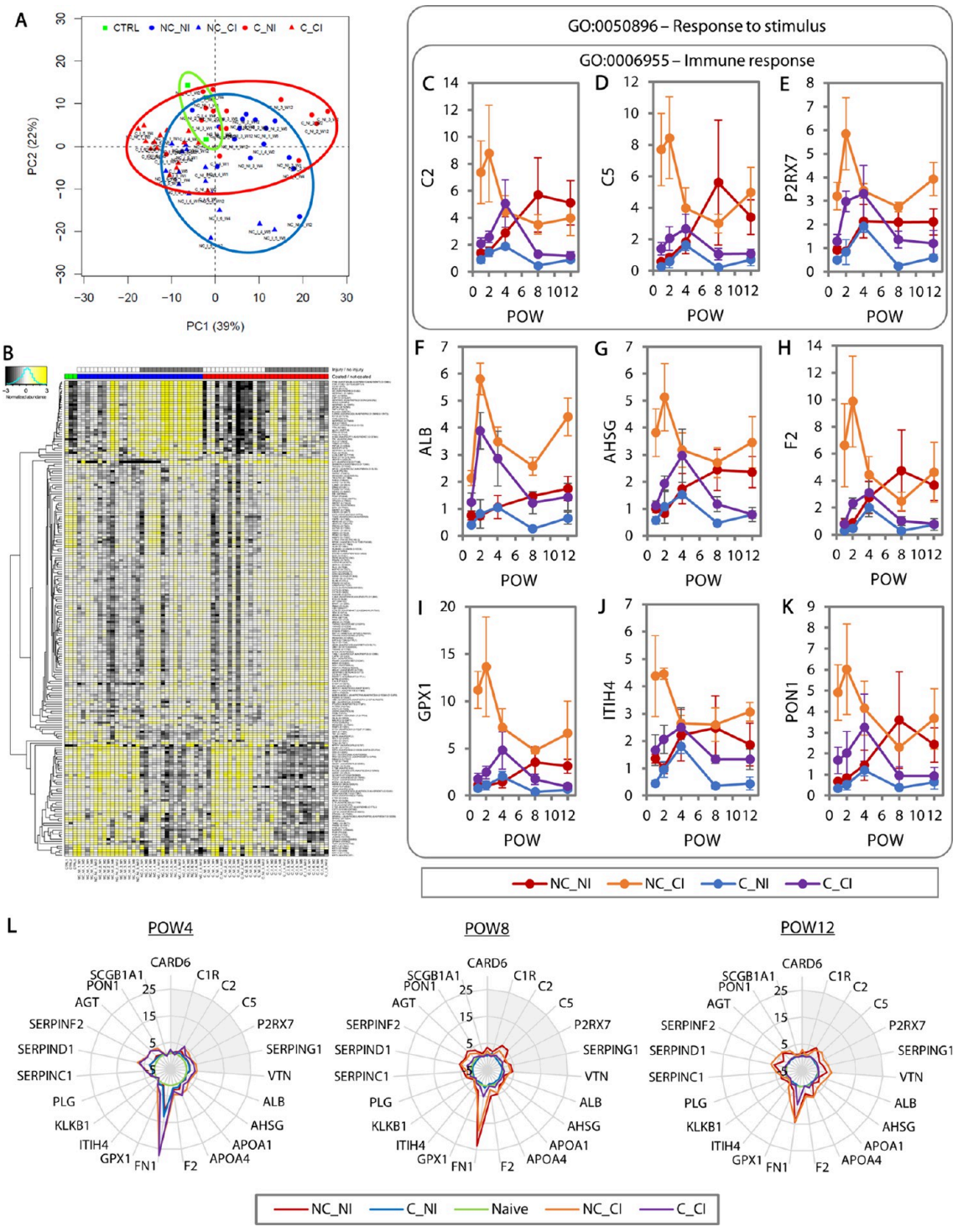

Figure 7. Tear proteomics analysis of responses to implantation with nHAp-coated and noncoated KPros across postoperative time points. (A) PCA plot indicates a more proximal clustering of tear proteins collected from eyes with coated KPros to the control tears of naive eyes when compared to the noncoated KPro implanted eyes whether in the noninjured (shortened as NI) or chemically injured situations (shortened as CI). (B) There were 621 tear proteins detected, but only 49 and 9 were differentially downregulated and upregulated, respectively, in the eyes implanted with coated KPros relative to the noncoated group. Twenty-three of the differentially downregulated proteins were associated with response to stimulus biological process (GO:0050896; $p = 3.3 \times 10^{-5}$). For example, complement 2 (C2) (C), C5 (D), purinergic receptor P2X 7 (P2RX7) (E), albumin (ALB) (F), alpha 2-HS glycoprotein (AHSG) (G), coagulation factor II (F2) (H), glutathione peroxidase 1 (GPX1) (I), interalpha-trypsin inhibitor heavy chain 4 (ITIH4) (J), and paraoxonase (PON1) (K). Out of the 23, 9 proteins were also involved in immune response (GO:0006955; $p = 3.8 \times 10^{-4}$), for instance, C2, C5, and P2RX7. (L) Radar maps revealed the similarity in the collective expression of proteins associated with response to stimulus and immune response (shaded area) at week 4 after either KPro implantations in both noninjury and chemical injury situations. The proteins were expressed at higher levels in the subsequent follow-up periods in the eyes with noncoated prostheses. However, these proteins were reduced in the presence of nHAp coating after week 8 and were close to the naive state after 12 weeks. Data are presented as mean ± SE ($n = 3$ in each group). NC = noncoated. C = coated. POW = postoperative week.

https://doi.org/10.1021/acsami.4c04077
ACS Appl. Mater. Interfaces 2024, 16, 25892−25908

weeks after the injury induction (Figure 3A). The corneal surface remained covered by CK4-positive conjunctival epithelial cells at 4 weeks after KPro implantation (Figure 3A). Slit-lamp images revealed increasing severity of corneal opacity and neovascularization over 12 weeks in both eyes implanted with coated and noncoated prostheses (Figure 3B). Conjunctival hyperemia peaked at week 4 and did not seem to subside in both cases. Although the fluorescein staining severity appeared similar, the staining area improved at a more rapid rate, following the implantation of coated KPro than the noncoated KPro. Similar to the noninjured corneas, the differences in all scoring categories and total score between the noncoated and coated KPros did not reach statistical significance levels (Figure 3C−K and Table S1), but the differences were greater in the chemically injured situations than in the noninjured corneas. Categories that produced median differences ≥1 included 1 conjunctival swelling score higher at week 4 (Figure 3D and Table S1), 1 pannus grade greater at week 1 (Figure 3G and Table S1), 1 aqueous flare score higher at weeks 2, 8, and 12 (Figure 3H and Table S1), and 1 and 1.5 higher fluorescein severity scores at weeks 2 and 12, respectively (Figure 3I and Table S1) in the eyes with noncoated KPros than those with coated implants. The eyes with noncoated KPros scored 1.5 higher total scores at weeks 1 and 2, and 4 and 5 greater total scores at weeks 8 and 12, respectively, than those with coated devices (Figure 3K and Table S1). The clinical grading outcomes suggested that nHAp conferred a more significant clinical benefit and milder ocular surface reactions with KPro implantation following chemical injury.

2.3. Tissue Adhesion on PMMA. The clinical benefit of nHAp coating carried over to the tissue adhesion. Using anterior segment-optical coherence tomography (AS-OCT) images taken in four planes (Figure 4A), the percentage area of attachment of the KPro (coated or noncoated) was calculated at each postoperative observation point. In noninjured corneas, percentage attachment was significantly greater in nHAp-coated KPros at postoperative weeks 2 ($p = 0.021$) and 12 ($p = 0.012$) but was otherwise similar across observation points (Figure 4B and Table S2). In some meridional scans, for example, at 0−180 and 45−225° scan angles of the cornea with noncoated KPro at week 12, tissue thinning and detachment were noticeable. The difference in tissue attachment propensity was starker in the chemical injury model, where the attachment was substantially greater at every observation point for nHAp-coated KPros compared to the nontreated devices (Figure 4C and Table S2). In the earlier time points, the detachment, showing up as a void on the AS-OCT scan, was typically observed in the corner of the dome-shaped front segment and first stem segment of the PMMA optical cylinder. The detachment became larger, and in some rabbits, the stroma was completely detached from the PMMA dome.

Corneas were excised 12 weeks after implantation to further quantify attachment. The locking ring and backplate were carefully removed before a monitored, and increasing force was applied until the optical cylinder was detached from the surrounding corneal tissue (Figure 5A). The tests demonstrated that nHAp-coated KPros required greater force to displace and detach them from the corneas into which they were implanted when compared with noncoated KPros, in both noninjured and chemically injured corneas (Figure 5B). Although the differences were not statistically significant, the force at failure was recorded at ∼36.9 and ∼22.6% higher with the coating than without it in the noninjured and chemically injured eyes, respectively (Figure 5C and Table S3). The overall work done was ∼23.5 and ∼31.8% greater to detach corneal tissues from the coated PMMA in the noninjured and chemically injured eyes, respectively (Figure 5D and Table S3).

The SEM of the detached PMMA from both noninjured and chemically injured eyes revealed the presence of a mixture of cuboidal and cornified epithelial cells on the noncoated PMMA surfaces, suggesting the infiltration of the epithelial cells into the gaps between the optical cylinders and tissues from poor attachment (Figure 5E). On the coated optical cylinders, although cuboidal epithelial cells could also be seen, the surface was predominantly attached with bundles of collagen fibers (Figure 5E). On these optical cylinders, in areas that were not masked by the collagen fibers (pointed by arrows), the nHAp could still be seen, suggesting its retention even after the push-in mechanical tests (Figure S1). The SEM also showed the difference in the attachment failure mode, where with coating, other than the tissue-nHAp adhesion, the tissue cohesiveness also played a role in the strength of the attachment. In contrast, without coating, the attachment failure was all attributed to the tissue-PMMA adhesion.

2.4. Fibrotic Responses to AuroKPro Implantation. Immunohistochemistry experiments were conducted on the detached corneal tissues to analyze fibrosis in response to KPro implantation and to potentially unravel the mechanism of action behind the improved attachment conferred by the nHAp coating (Figure 5A). All typical corneal fibrosis markers, such as fibronectin (Figure 6A), CD90 or Thy-1 (Figure 6B), collagen 3A1 (Figure 6C), and α-smooth muscle actin (α-SMA) (Figure 6D), were expressed in the tissues adjacent to the PMMA optical cylinders (now removed), representing usual tissue responses to the KPro implantation.[34,35] These markers, namely, fibronectin, CD90, and α-SMA, were not present in naïve corneas, while collagen 3A1 was expressed weakly (Figure S2). In the noninjured eyes, the fibronectin, CD90, collagen 3A1, and α-SMA were more abundant with noncoated KPros than with the coated prostheses but the differences were not statistically significant (Figure 6A−D and Table S4). However, the expression of fibronectin ($p = 0.036$), collagen 3A1 ($p = 0.032$), and α-SMA ($p = 0.039$) were markedly greater in corneas implanted with noncoated KPros than those implanted with coated prostheses following chemical injury. CD90 was only weakly expressed and appeared to be at a similar level with or without nHAp coating.

2.5. Tear Proteomics. Tear proteomics could provide noninvasive screening for protein mediators of ocular surface responses to corneal implants.[36,37] It also allowed investigation into temporal tissue responses without having to sacrifice animals at multiple time points. The PCA score plot indicated clustering of tear proteins collected from eyes with coated KPros closer to the control tears from naïve eyes when compared to the samples from noncoated KPro-implanted eyes whether in the noninjured or chemically injured conditions (Figure 7A). In total, 621 common tear proteins were identified in all the rabbits. There were 49 differentially downregulated proteins and 9 upregulated proteins in the coated group relative to the noncoated group (Figure 7B). Twenty-three of the downregulated proteins (46.9% of the differentially downregulated proteins) were collectively involved in the response to stimulus (GO:0050896; $p = 3.3 \times 10^{-5}$) (Table S5). They were caspase recruitment domain family member 6 (CARD6) (Figure S3A), complement 1R (C1R) (Figure S3B), complement 2 (C2) (Figure 7C), complement 5 (C5) (Figure 7D), purinergic

https://doi.org/10.1021/acsami.4c04077
ACS Appl. Mater. Interfaces 2024, 16, 25892−25908

receptor P2X 7 (P2RX7) (Figure 7E), serpin G1 (SERPING1) (Figure S3C), vitronectin (VTN) (Figure S3D), albumin (ALB) (Figure 7F), alpha 2-HS glycoprotein (AHSG) (Figure 7G), apoliporotein A1 (APOA1) (Figure S3H), APOA4 (Figure S3I), coagulation factor II (F2) (Figure 7H), fibronectin (FN1) (Figure S3K), glutathione peroxidase 1 (GPX1) (Figure 7I), interalpha-trypsin inhibitor heavy chain 4 (ITIH4) (Figure 7J), kallikrein B1 (KLKB1) (Figure S3H), SERPINC1 (Figure S3I), plasminogen (PLG) (Figure S3J), SERPINF2 (Figure S3K), SERPIND1 (Figure S3L), angiotensinogen (AGT) (Figure S3M), paraoxonase (PON1) (Figure 7K), and secretoglobin 1A1 (SCGB1A1) (Figure S3N). In noninjured eyes, at week 4, the collective expression of these proteins—determined by area-under-curve in the radar map—with the noncoated KPros was 22.9 ± 17.2% higher than that in naïve eyes. This was similar to the tear proteomic response to stimulus with coated KPros (33.5 ± 22.1% of naïve; $p = 0.724$) (Figure 7L). These proteins were upregulated further at weeks 8 (122.8 ± 38.2% of naïve) and 12 (178.1 ± 76.5% of naïve) in the eyes with noncoated KPros (Figure 7L). In contrast, the protein expression was reduced with the coated KPros at both weeks 8 (−26.6 ± 5.8% of naïve; $p = 0.018$ vs noncoated) and 12 (−9.9 ± 13.1% of naïve; $p = 0.073$ vs noncoated). A similar tear proteomic response to stimulus was seen in the chemically injured rabbits, where the collective protein expression with the noncoated devices (93.0 ± 17.0% higher than naïve) was similar to that with the coated devices (101.8 ± 47.9%; $p = 0.870$) at week 4 (Figure 7L). The proteins were continually upregulated in the eyes with the noncoated KPros (151.7 ± 40.5% of naïve at week 8 and 246.5 ± 79.3% of naïve at week 12), whereas, in the eyes with coated prostheses, the protein level had returned close to the naïve state at week 12 (1.1 ± 13.0% of naïve; $p = 0.038$ vs noncoated), which was a further downregulation from week 8 (13.3 ± 13.6%; $p = 0.032$ vs noncoated) (Figure 7L).

Nine of the aforementioned proteins were involved in immune response (GO:0006955; $p = 3.8 \times 10^{-4}$) (Table S5), namely, APOA1, APOA4, CARD6, C1R, C2, C5, P2RX7, SERPING1, and VTN. The pattern of collective expression of these proteins reciprocated the proteins associated with response to stimulus, where the levels of secretion were similar at week 4 post-KPro implantation in either noninjured eyes ($p = 0.650$) or chemically injured eyes ($p = 0.838$) (Figure 7L). However, in the subsequent follow-up periods, these proteins were continually upregulated in the eyes with noncoated prostheses in the noninjury eyes (from 131.2 ± 53.8% of naïve at week 8 to 262.5 ± 124.0% of naïve at week 12) and chemical injury eyes (from 192.0 ± 60.1% of naïve at week 8 to 353.3 ± 83.3% of naïve at week 12). A contrasting immune response was seen in the eyes with coated prostheses, where the associated protein levels were reduced after 8 weeks to a near naïve state. The protein expression was −6.2 ± 27.2% of naïve in the noninjured eyes ($p = 0.102$) and −21.7 ± 24.7% of naïve in the chemically burned eyes ($p = 0.012$) at week 12. Out of nine differentially upregulated proteins, only two of them were significantly associated with biological processes. They were UDP-glucose 6-dehydrogenase (UGDH) (Figure S4A) and fatty acid binding protein 5 (FABP5) (Figure S4B), which were associated with organic acid biosynthetic process (GO:0016053; $p = 5.2 \times 10^{-2}$) and carboxylic acid biosynthetic process (GO:0046394; $p = 5.2 \times 10^{-2}$).

3. DISCUSSION

In this study, after optimization, we successfully applied a dip-coating strategy—previously tested on PMMA sheets and rods—to lay down a uniform nHAp coating on the PMMA surface of the optical cylinders of clinical-grade AuroKPro.[25,31] Preclinical investigations indicated excellent functionality and biocompatibility across the postoperative monitoring period, and nHAp coating conferred superior clinical outcomes in corneas, which were chemically injured before implantation. This improvement was related to the superior biointegration into surrounding corneal tissue conferred by the nHAp coating, evidenced by visualized surface apposition and physical forces required to detach the KPros from recipient corneas. Improved integration with the nHAp coating was facilitated by a lower magnitude of fibrotic response and volume of secretion of tear proteins associated with responses to immunogenic stimuli, evidencing how the coating confers greater biocompatibility than an unmodified PMMA surface.

Considering the cohort of patients that require these KPros is typically in low-income countries, to keep the cost of the KPro low, we opted for a relatively inexpensive surface engineering technique that only requires a dip-coater, plasma processing system, and probe sonicator to implement. Alternative methods of applying a HAp coating, including plasma spraying and magnetron sputtering, were considered.[29,30] These techniques, however, require expensive capital outlay to set up. From the technical aspect, the techniques are not suitable for low melting temperature and brittle polymers, like the PMMA, and are difficult to apply on small surface areas, like the AuroKPro's PMMA optical cylinder. Arguments can be made about surface modifications with peptides, such as RGD (Arg-Gly-Asp) or elastin-like recombinamers,[38,39] and surface chemistry alterations with radio frequency plasma (3-aminopropyl)-triethoxysilane (3-APTES), L-3,4-dihydroxyphenylalanine (L-DOPA), or NaOH,[40−42] which are nonthermal and nonline-of-sight methods. However, we opted to use nHAp for its likely longer-lasting effects than peptide or chemical surface modification, which can exhibit premature degradation due to abnormal protease and immune activity in ocular surface disease.[43,44]

We made a minor modification to the dip-coating protocol from the previously described approach used for PMMA rods, because it was apparent that nHAp did not adhere to the AuroKPro's PMMA optical cylinder.[25] The PMMA was exceptionally hydrophobic, evidenced by the high surface tension visible when the optical cylinder was lowered into the dip-coating solution. We posited that additives might have been added during the manufacturing process—a common practice in the industry—resulting in changes to the surface properties of the PMMA.[45] This was confirmed by the KPro manufacturer, although the specifics of the additives could not be disclosed. We added additional steps before nHAp dip-coating: increasing the hydrophilicity of the PMMA with 1 M NaOH and "softening" the surface for the nHAp to adhere through a series of dipping in chloroform and PMMA-containing chloroform. This surface priming facilitated immobilization of nHAp, with complete coverage of the PMMA surface observed after three 5 s dips.

The initial focus on clinical outcomes, notably in eyes subjected to chemical injury, underscores the translational relevance of the nHAp-coated AuroKPro for treating challenging conditions such as total LSCD. The clinical outcomes in the noninjured rabbit eyes suggested an absence of overwhelming

https://doi.org/10.1021/acsami.4c04077
ACS Appl. Mater. Interfaces 2024, 16, 25892−25908

differences in noninjured corneas, ensuring the safety of the coating under baseline conditions and its clinical applicability. In noninjured corneas, the most obvious disparity between nHAp-coated and noncoated prosthesis was the fluorescein staining severity and area. Staining tracks in the tissue−PMMA interface after noncoated KPro implantation were suggestive of a poorer seal between the two surfaces. Clinical benefits of the nHAp coating were more apparent in clinically injured corneas, quantified by aqueous flare at weeks 2, 8, and 12, as well as fluorescein staining at weeks 2 and 12. The fluorescein area was also consistently larger in eyes that received noncoated KPros at all follow-up points. These advantages were reflected by lower total Hackett−McDonald scores of injury at weeks 8 and 12 for eyes that received coated KPros rather than uncoated KPros.

At 3 months postoperation in chemically injured eyes, the stromal tissues were well adhered to the nHAp coating. On AS-OCT, markedly superior tissue apposition to the coated PMMA optical cylinders was observed at 98.7 ± 2.1 area vs 76.2 ± 10.2% area in the eyes with noncoated PMMA (p = 0.001). Superior tissue apposition translated to tissue adhesion (~22.6% greater force and ~31.8% greater work required to detach the tissue) when we subjected the corneas that were still attached to the PMMA optical cylinders to mechanical push-in tests, although the difference did not reach a statistically significant level. This may be because, although extreme care was taken when separating the corneal tissues that had grown into and around the PMMA backplates, trimming may have caused micromovements resulting in the adhesion of tissue to the optical cylinder. Nevertheless, clear differences in tissue attachment were shown by the presence of collagen fibrillar bundles adherent to the nHAp coating after mechanical tests, suggestive of a direct interaction between the tissue and coating. No such adherent tissue was observed with uncoated PMMA surfaces. We noticed patches of epithelial cells on the PMMA with no presence of collagen fibers, which suggested that these cells migrated into the space of the looser tissue attachment: a phenomenon reported before in KPro patients.[46] As similar patterns of tissue adhesion were observed in noninjured eyes, we concluded that the sequelae of chemical injury do not affect the efficacy of the nHAp coating.

The immunohistochemistry and tear proteomics experiments interrogating fibrotic responses provided mechanistic insight into the clinical and mechanical benefits conferred by the nHAp coating. Downregulation of fibrotic markers such as fibronectin, collagen, 3A1, and α-SMA, in corneas implanted with coated KPros (particularly following chemical injury), substantiated previously described findings that corneal stromal cells elicited attenuated fibrotic responses in the presence of nHAp coating.[25] Increased expression of fibrosis markers is an early sign of nonadherent fibrous capsule formation which typically encapsulates bioinert material such as PMMA.[11] While these markers were also present in the corneal stroma following coated KPro implantation, expression was much attenuated and may reflect a usual wound healing response to surgery.

A further advantage of nHAp coating was revealed by tear proteomic analysis: at an earlier time point (postoperative week 4), the collective expression of the differentially expressed proteins associated with response to stimulus and immune response was similar regardless of the coating in both noninjured and chemically injured eyes. However, while these proteins continued to be upregulated to higher levels at weeks 8 and 12 in the eyes with noncoated prostheses, they were continuously reduced in the presence of the nHAp coating. Taking the proteins associated with response to stimulus as an example, their collective expression increased from 22.9 ± 17.2% of naïve at week 4 to 178.1 ± 76.5% higher than naive at week 12 in the noninjured eyes. In a similar trend, these proteins increased from 93.0 ± 17.0% of naïve at week 4 to 246.5 ± 79.3% higher than naïve at week 12 in injured eyes. In contrast, in the eyes with coated KPros, these protein secretions were reduced to a near naïve state after 12 weeks whether in the injured or noninjured situations (1.1 ± 13.0% and −9.9 ± 13.1% of naïve in injured and noninjured eyes, respectively). The earlier downregulation of tear proteins associated with response to stimulus and immune response implied a less stimulant and anti-inflammatory milieu induced by the nHAp coating. Similar antifibrosis and anti-inflammatory effects of nHAp have also been demonstrated in human dermal fibroblasts and Tenon's fibroblasts.[22,24] These molecular dynamics contribute to overall homeostasis and favorable outcomes, which eventually lead to superior biointegration observed with coated prostheses.

Besides the biological effects discussed above, it was also likely that the superior biointegration was attributed to the changes in the surface properties conferred by the nHAp coating. Because of the relatively small surface area covered by nHAp on the AuroKPro's PMMA optical cylinder, it was challenging to conduct an in-depth surface characterization. Much of the surface characterization has been carried out on PMMA sheets in our previous research articles.[27,31,47] First, the nHAp conferred increased hydrophilicity in a water contact angle test (18.7 ± 2.7 vs 68.1 ± 1.1° on uncoated PMMA).[47] Second, the nHAp coating provided a textured surface with an average R_q of 92.5 ± 10.5 nm, making it more conducive for tissue adhesion than the uncoated PMMA with an average R_q of 1.5 ± 0.3 nm.[31] With the nHAp preannealed, the coating process did not involve any heat and resulted in stoichiometric apatite layer on EDX and the maintenance of the fidelity of the HAp phase and crystallinity on graze incidence-X-ray diffraction.[27,31] Moreover, with the nHAp well anchored in the PMMA, the coating did not delaminate even after a tape adhesion test with Scotch tape (with 1.23 N/cm adhesion rating).[31] The cumulative effects of the physical and chemical properties of the nHAp coating produced approximately fivefold better collagen type I molecule adhesion on quartz crystal microbalance and approximately sixfold better corneal stromal fibroblast attachment efficiency.[31]

The aforementioned factors are advantages of the nHAp dip-coating method over the conventional biomimetic HAp coating method via the incubation in simulated body fluid (SBF).[27] The biomimetic approach offers simplicity in method, eliminates the need for specialized equipment, and allows the coating of porous or intricately shaped substrates and the inclusion of growth factors, proteins, or DNA. However, the scarcity of clinical applications indicates a stagnation in translational efforts, potentially influenced by various factors. Inconsistencies in coating outcomes, such as varying crystallinity levels, phases of calcium phosphate (CaP), and mineral purity, have been observed in studies.[21,27,41,48,49] Inconsistent coating properties across reports may stem from differing surface functional groups required to induce efficient apatite nucleation, as well as fluctuations in SBF pH and temperature during preparation, storage, or coating.[50] CaP deposition in SBF typically takes days to weeks, and the coating, anchored by ionic bonds, is prone to delamination, particularly on devices subjected to tangential or horizontal forces.[41] Hence, upscaling a lengthy and inconsistent process is impractical from a pragmatic standpoint.

https://doi.org/10.1021/acsami.4c04077
ACS Appl. Mater. Interfaces 2024, 16, 25892−25908

4. CONCLUSIONS

This study was limited by a small sample size and a relatively short postoperative follow-up period. Although KPro extrusion is a common problem in human patients, mean time to failure tends to be in the order of years, rather than weeks.[51,52] Limbal stem cell deficiency, neovascularization, edema, and scarring associated with chemical burns and other severe corneal pathology are thought to contribute to KPro failure, and higher failure rates are observed following KPro for these indications rather than to replace a previous graft.[18,51] As short-term rates of extrusion are low in rabbit and man, mechanical and biological markers of extrusion risk—assessed in this study—may be the best way to evaluate surface engineering approaches in the preclinical setting.[51,53] Although our follow-up period was too short to observe complete KPro extrusion and some test outcomes did not reach statistical significance, even in the total LSCD model, we noticed several clear disparities in the rabbits implanted with noncoated prostheses after 12 weeks: (1) The persistent epithelial defect, indicated by the fluorescein staining, was more severe; (2) tissue apposition and mechanically tested adhesion were lower; (3) fibrosis was substantially more severe; and (4) tear protein secretion in response to stimuli of injury and KPro implantation was significantly greater than in animals that received coated KPros.

In summary, augmentation of the AuroKPro with nHAp coating of the PMMA optical cylinder improved clinical outcomes and device biointegration in rabbits undergoing KPro following ocular chemical burns, through attenuation of fibrotic and immune responses indicated by a less immunogenic response to the nHp-coated surface. Clinical studies are warranted to trial nHAp-coated KPros in human patients and should be sufficiently powered to detect clinically meaningful decreases in the rates of device failure and complications.

5. EXPERIMENTAL SECTION

5.1. Immobilization of Nanohydroxyapatite on the PMMA Optical Cylinder. Twenty-five clinical-grade AuroKPros were kindly provided by Aurolab (Madurai, India) for the study. Each set of AuroKPro included a PMMA optical cylinder, PMMA backplate, and titanium locking ring, packed individually and presterilized with ethylene oxide gas. Fifteen of the optical cylinders were subjected to nHAp coating (Figure 1A). The surface of the optical cylinder was first activated in 1 N NaOH (Sigma-Aldrich, St. Louis, Missouri) for 1 h at 50 °C, washed in copious amounts of deionized water, and dried overnight at 37 °C. Immobilization of the nHAp on the PMMA optical cylinder was achieved via a dip-coating approach utilizing an automated KSV NIMA dip-coater (Biolin Scientific, Stockholm, Sweden). The lowering and withdrawal speeds were set at 180 mm/min. The PMMA optical cylinder was carefully masked with silicone as such that the curved anterior-most and the posterior-most surfaces (where the light path would traverse) would not be affected by the dip-coating process. The sample was first dipped in chloroform solution (Merck Millipore, Burlington, Massachusetts), 2.5% (w/v) PMMA (MW 120,000; Sigma-Aldrich) in chloroform solution, and nHAp-containing dip-coating solution for 5 s each. The nHAp-containing dip-coating solution was prepared by mixing 20% (w/v) 60 nm nHAp (MKnano, Mississauga, Canada) in chloroform containing 5% (w/v) PMMA. A probe sonicator (Qsonica, Newton, Connecticut) was then used to disperse the dip-coating solution for 30 min at an amplification level of 50% with a 5 s pause after every 5 s sonication. Following the automated dip-coating sequence, the lightly coated optical cylinder was air-dried for 30 min to allow for chloroform evaporation and nanoparticle settlement at the surface. To fully cover the surface, the optical cylinder was then subjected to two more cycles of dip-coating (only in nHAp-containing dip-coating solution) and air drying. After the masking was removed, the coated sample was dried overnight at 37 °C.

The following day, the optical cylinder was subjected to oxygen plasma treatment to remove contaminants and PMMA that had masked the nHAp surface. The oxygen plasma etching of the PMMA mask revealed more nHAp to the surface.[31] The optical cylinder was placed anterior side down in a Covance plasma system (Femto Science, South Korea). The chamber was purged with oxygen gas at a flow rate of 20 standard cubic centimeters per minute (sccm). The sample was then treated with radio frequency oxygen plasma with 200 W power for 5 min. After plasma discharge, the sample was washed with 70% ethanol three times, 15 min each, followed by copious amounts of distilled water, and dried in a 37 °C incubator. Finally, the coated optical cylinder was sterilized with UV−C light.

5.2. Transparency of the Optical Cylinder. The optical transparency of noncoated and coated PMMA optical cylinders (n = 3 in each group) was analyzed to determine whether the visual axis of the optic was affected by the dip-coating. The percentage light transmittance was converted from absorbance measured across visible-light wavelengths (390−700 nm) with a Tecan Infinite 200 microplate reader (Maennedorf, Switzerland).

5.3. Coating Surface Morphology and Elemental Composition Analysis. The surface morphology of the coated PMMA optical cylinder (n = 3) was analyzed by SEM. In brief, the sample was mounted on a stub secured by carbon adhesive tape and sputter-coated with a 10 nm-thick layer of platinum and examined with a JSM-7600F microscope (JEOL, Tokyo, Japan) at an accelerating voltage of 5 kV. Surface elemental composition was assessed by EDX spectroscopy attached to the SEM.

5.4. Implantation of Coated AuroKPro in Rabbit Cornea. Sixteen 12- to 15-week-old New Zealand White rabbits were procured from InVivos, Singapore. The surgical protocol was approved by the Institutional Animal Care and Use Committee of SingHealth-Duke-NUS, Singapore (2016/SHS/1151), and conformed to the guidelines set by the Association for Research in Vision and Ophthalmology for the use of animals in ophthalmic and vision research. The implantation procedure in the rabbits simulated the implantation of AuroKPro in patients. All rabbits underwent cataract extraction surgeries with a standard phacoemulsification procedure using the White Star Signature phacoemulsification system (Abbott Medical Optics, Santa Ana, California) 1 week before KPro implantation in the noninjured model or 1 week before alkali burn in the chemical injury model. The donor corneas were harvested from other rabbits that underwent unrelated procedures. Briefly, the corneas were marked with an 8 mm-diameter biopsy punch and excised with Vannas scissors (Duckworth & Kent, Baldock, UK). The corneas were preserved in Optisol-GS (Bausch+Lomb, Bridgewater, New Jersey) at 4 °C for 10−14 days. The KPros were implanted in two rabbit models (Figure 2A): (1) noninjured model (naïve cornea; n = 8) and (2) chemically injured model (alkali burn cornea; n = 8). Only one eye of each rabbit was implanted with the prosthesis (the fellow eye was used as an untreated control). In the first model, four rabbits were implanted with coated KPros and four rabbits with noncoated KPros in naïve corneas. To prepare for the assembly of a KPro device, the donor cornea was trephined centrally with a 3 mm-diameter punch and then slid over the stem of the PMMA front plate (Video S1). The backplate was then positioned and locked on the stem such that the donor cornea became securely sandwiched between the front and back plates. Following KPro device construction, the recipient rabbit was anesthetized with xylazine (5 mg/kg intramuscularly; Troy Laboratories, Smithfield, Australia) and ketamine (50 mg/kg intramuscularly; Parnell Laboratories, Alexandria, Australia) and the eyelids cleaned with iodine and draped. The central cornea of the recipient was excised using an 8.0 mm trephine. The KPro construct was then placed in the recipient's eye and secured with 16 interrupted 11−0 nylon sutures (Johnson & Johnson, New Brunswick, New Jersey). After the procedure, the anterior chamber was reformed with Viscoat (Alcon, Fort Worth, Texas). Tobramycin and dexamethasone ointment (Tobradex, Alcon) was applied six times a day for the first month and tapered to four times a day until the end of the study. Corneal sutures were removed after 8 weeks.

https://doi.org/10.1021/acsami.4c04077
ACS Appl. Mater. Interfaces 2024, 16, 25892−25908

Table 1. Clinical Grading Categories and Description

grading	description
Conjunctival congestion	
0	normal: bulbar conjunctiva may appear pale pink without perilimbal injection. Small vessels associated with the dorsal and ventral rectus muscles may be seen at 12 and 6 o'clock positions.
1	mild: pink-to-red bulbar conjunctiva with some perilimbal injection at the upper and lower regions of the eye.
2	moderate: red bulbar conjunctiva with accompanying perilimbal injection encompassing at least 75% of the circumference of the perilimbal region.
3	severe: red-to-dark red bulbar conjunctiva with pronounced perilimbal injection. Vessels have extensive branching that is extended from the limbus to the fornix. Petechiae may be present in the conjunctiva.
Conjunctival swelling	
0	normal: no abnormal swelling of the conjunctival tissue.
1	minimal: bulbar conjunctival swelling above normal is observed focally, most commonly in the perilimbal region with no change in eyelid margin contour.
2	mild: bulbar conjunctival swelling above normal is observed diffusely but with no change in eyelid margin contour.
3	moderate: bulbar and palpebral conjunctival swelling is observed, resulting in eyelid eversion and/or misalignment. The eyelids can still be closed completely.
4	severe: bulbar and palpebral conjunctival swelling is severe to the extent of obscuring examination of the rest of the ocular surface and globe. Eyelid closure is incomplete with exposed bulbar and/or palpebral conjunctiva protruding.
Conjunctival discharge	
0	normal: no abnormal discharge.
1	mild: discharge is above normal and present on the surface of the eye or in the medial canthus, but not on the lids or hairs of the eyelids.
2	moderate: discharge is abundant, is easily observed, and has accumulated on the lids and around the hairs of the eyelids.
3	severe: discharge has been flowing over the eyelids, wetting the hairs of the eyelids and the skin around the eyes, past the orbital rim.
Aqueous flare (observation was supplemented with AS-OCT)	
0	normal: absence of visible light beam in the anterior chamber (no Tyndall effect).
1	mild: the Tyndall effect is barely discernible. The intensity of the light scattering in the anterior chamber is less than the intensity of the slit beam as it passes through the lens.
2	moderate: the Tyndall beam in the anterior chamber is easily discernible and is equal in intensity to the slit beam as it passes through the lens.
3	severe: the Tyndall beam in the anterior chamber is easily discernible. The intensity is greater than the slit beam as it passes through the lens.
Corneal opacity	
0	normal: clear with no haze or opacity.
1	minimal: the underlying anterior segment structures are visible, although corneal opacity is apparent to an experienced observer.
2	mild: the underlying anterior segment structures are visible, although there is a reduction in the ability to appreciate their detail.
3	moderate: there is a greater inability to see the details of the underlying anterior segment structures than with a score of 2, but the observer is still able to score aqueous flare, see iris vessels, and observe for a pupillary response.
4	severe: the underlying anterior segment structures cannot be seen.
Pannus	
0	normal: no corneal vascularization.
1	mild: vascularization is present but vessels have not penetrated beyond 2 mm axially.
2	severe: vascularization is present and vessels have penetrated ≥2 mm axially.
Fluorescein staining severity	
0	normal: absence of fluorescein staining.
1	slight: With diffuse illumination, slight multifocal punctate fluorescein staining.
2	mild: with diffuse illumination, distinct multifocal to coalescent punctate fluorescein staining.
3	marked: with diffuse illumination, fluorescein staining associated with focal or multifocal epithelial loss, but no stromal loss.
4	severe: with diffuse illumination, fluorescein staining associated with focal or multifocal epithelial and stromal loss.
Fluorescein staining area	
0	no area of fluorescein staining.
1	1−25% area of fluorescein staining.
2	26−50% area of fluorescein staining.
3	51−75% area of fluorescein staining.
4	76−100% area of fluorescein staining.

In the second rabbit model, four rabbits were implanted with coated KPros and four rabbits with noncoated KPros in alkali burn corneas. Three weeks before the KPro implantation, a chemical injury was created on the rabbit's ocular surface. A drop of proxymetacaine hydrochloride (Alcaine, Alcon) was applied to the experimental eye. Under anesthesia, a ring-shaped filter paper with an 11 mm inner diameter and 16 mm outer diameter, soaked with 1 N NaOH (Sigma-Aldrich), was placed on the ocular surface covering the limbus for 1 min. The ocular surface was then rinsed with 10 mL of 1× phosphate-buffered saline (PBS; 1st BASE, Singapore). The remaining central corneal epithelial cells were scraped off with a Beaver blade #64 (BD Medical, Waltham, Massachusetts). The KPro assembly and implantation and postoperative care were carried out similarly as in the first rabbit model, as described above.

5.5. Postoperative Examinations. Postoperative examinations were performed on weeks 1, 2, 4, 8, and 12 following the implantation of AuroKPro. First, slit-lamp photography using a Righton MW50D (Righton, Tokyo, Japan) was performed to examine the gross appearance of the cornea and conjunctiva. Fluorescein staining was also performed by applying a drop of 1% fluorescein sodium (Bausch +Lomb) on the cornea. The extent of the staining was then viewed with the blue light of the slit lamp. Clinical outcomes were graded based on the modified Hackett−McDonald scoring system.[54] Eight different categories (Table 1), namely, conjunctival congestion, conjunctival swelling, conjunctival discharge, aqueous flare, corneal opacity, pannus, and fluorescein staining severity, and area, were graded by a masked observer. AS-OCT with a Visante system (Carl Zeiss Meditec, Jena, Germany) was then performed to examine cross sections of the cornea.

https://doi.org/10.1021/acsami.4c04077
ACS Appl. Mater. Interfaces 2024, 16, 25892−25908

Line scans at four different meridians, 0−180, 45−225, 90−270, and 135−225°, were captured to assess the tissue attachment at various contact points along the circumference of the PMMA optical cylinder.

5.6. Impression Cytology of the Ocular Surface. Impressions of rabbit conjunctival and/or corneal epithelium (n = 4 in each group) were collected on the filter papers of Millicell cell culture inserts (Merck Millipore). The epithelial cells on the filter papers were then fixed in 4% paraformaldehyde (Sigma-Aldrich), washed in 1× PBS (1st BASE), blocked in 4% bovine serum albumin (BSA; Sigma-Aldrich), and incubated with mouse monoclonal antibodies against CK3 (Abcam, Cambridge, UK) and CK4 (OriGene Technologies, Rockville, Maryland) overnight. After washing in 1× PBS, the sections were incubated with either goat antimouse Alexa Fluor 488 or Texas Red-X secondary antibodies (Thermo Fisher Scientific). The sections were then counterstained with DAPI (Santa Cruz Biotechnology, Dallas, Texas) and viewed with an AxioImager Z1 microscope (Carl Zeiss, Oberkochen, Germany).

5.7. Tissue Adhesion Strength Test. The tissue adhesion strength test was conducted after removing the locking ring and backplate from the KPro assembly (n = 4 in each group) (Figure 5A). Following animal euthanasia, the cornea (with AuroKPro still attached) was excised from the rabbit eye. The titanium locking ring was first removed from the posterior of the cornea by bending it out of place with a pair of forceps. Before the removal of the PMMA backplate from the KPro assembly, the corneal tissue that was attached to it was carefully severed with Vannas scissors. The remaining KPro components were subjected to a mechanical push-in test with a universal tensile tester (Chatillon, Largo, Florida). The KPro was mounted with the anterior of the PMMA optical cylinder down in a customized adapter. A 2 mm-diameter steel rod, attached to the load cell, would then push the optical cylinder until it was completely detached from the cornea. Maximum force at failure was reported and the area under the force−displacement curve was determined to measure the work done to detach the tissue.

5.8. Adhesion Failure Assessment and Visualization. Following the mechanical push-in test, the now detached PMMA optical cylinder was subjected to SEM (Figure 5A). The sample was fixed in 2.5% glutaraldehyde (Sigma-Aldrich) in 0.1 M sodium cacodylate (Merck Millipore) overnight at 4 °C and postfixed in 1% osmium tetroxide (Electron Microscopy Sciences, Hatfield, Pennsylvania) for 2 h at room temperature. The sample was then dehydrated in increasing concentrations of ethanol (Merck Millipore), followed by critical point drying in a Leica EM CPD300 (Leica Microsystems) and mounting on a sample stub with a carbon adhesive tab. The surface of the optical cylinder was finally coated with 15 nm-thick gold in a Leica EM ACE200 sputter coater (Leica Microsystems) and imaged with a FEI Quanta 650 FEG microscope (FEI Company, Hillsboro, Oregon).

5.9. Fibrotic Responses of Recipient's Cornea. The detached cornea (n = 4 in each group) was subjected to immunofluorescence staining (Figure 5A). It was fixed in 4% paraformaldehyde (Sigma-Aldrich) overnight and then embedded in the OCT cryo-compound (Leica Biosystems). Serial 8 μm-thick cryosections were cut with a Microm HM525 cryostat (Thermo Fisher Scientific, Waltham). The sections were washed in 1× PBS (first BASE), blocked in 4% BSA (Sigma-Aldrich), and incubated with mouse monoclonal antibodies against cellular fibronectin (clone DH1, Sigma-Aldrich), α-SMA (clone 1A4, Agilent Technologies, Santa Clara, California), and CD90 (clone OX7, Santa Cruz Biotechnology) and goat polyclonal antibody against collagen type IIIA1 (COL3A1) (Southern Biotech, Birmingham, Alabama) overnight. After washing, the sections were incubated with either goat antimouse Alexa Fluor 488 or rat antigoat Alexa Fluor 488 secondary antibodies (Thermo Fisher Scientific). The sections were then counterstained with DAPI (Santa Cruz Biotechnology) and viewed with an AxioImager Z1 microscope (Carl Zeiss). Serial 10× magnification images of the cornea were taken, stitched together, and presented to show the width of the cornea from one periphery to another. The antibody staining intensity was analyzed by measuring the Integrated Density of the Alexa Fluor 488 signal, after conversion to 8-bit grayscale, with ImageJ version 1.53t (National Institute of Health, Bethesda, Maryland).

5.10. Tear Proteomics. Rabbit tear samples (n = 3 in each group) were collected at weeks 1, 2, 4, 8, and 12 with Schirmer's strips. Tear proteins from a finely cut Schirmer's strip were extracted with 100 μL of 50 mM ammonium bicarbonate (per strip; Sigma-Aldrich) at 1300 rpm at room temperature for 1 h, and the protein concentration was measured. The protein sample (100 μg) was applied for SWATH-MS, and a spectral library was established as previously described.[55] The digested sample was reconstituted in a loading buffer (0.1% formic acid, 2% acetonitrile in water), and the iRT standard (Biognosys, Switzerland) was spiked. Sample analysis was performed using an UltiMate 3000 nanoLC system (Dionex, Thermo Fisher Scientific) coupled with AB SCIEX 5600 TripleTOF (AB SCIEX, Framingham, Massachusetts).

SWATH proteomics data were processed with Spectronaut (Biognosys, Schlieren, Switzerland). The relative quantitation data collected from eyes with coated KPros versus noncoated KPros at different time points were compared. Differential protein expression was defined with linear models for microarray data (LIMMA) algorithm with $\log_2$ FC > 0.58 or <−0.58, and $p < 0.05$.[56] Gene Ontology (GO) term analysis to identify enriched biological processes was done by inputting a database to web-based DAVID Bioinformatics 2021 (National Institutes of Health).[57]

5.11. Statistical Analysis. All data were expressed as mean ± standard error of the mean (SE). Statistical differences in clinical grading outcomes between noncoated and coated KPro groups were analyzed with the Mann−Whitney U test. The differences in the continuous data gathered from noncoated and coated KPro groups were assessed with the independent sample t test. All statistical analyses were performed with SPSS version 17.0 (IBM, Armonk, New York). Comparisons yielding a p value less than 0.05 were considered statistically significant.

■ ASSOCIATED CONTENT

Supporting Information

The Supporting Information is available free of charge at https://pubs.acs.org/doi/10.1021/acsami.4c04077.

High-magnification SEM images of nHAp-coated surfaces after mechanical push-in tests, immunofluorescence staining of naïve rabbit corneas, additional differentially expressed tear proteins; and data sets used to generate graphs in the main text (PDF)

AuroKPro implantation in rabbit cornea (MP4)

■ AUTHOR INFORMATION

Corresponding Authors

Jodhbir S. Mehta − *Tissue Engineering and Cell Therapy Group, Singapore Eye Research Institute, Singapore 169856, Singapore; Singapore National Eye Centre, Singapore 168751, Singapore; Ophthalmology and Visual Sciences Academic Clinical Programme, Duke-NUS Medical School, Singapore 169857, Singapore*; Email: jodhbir.s.mehta@singhealth.com.sg

Andri K. Riau − *Tissue Engineering and Cell Therapy Group, Singapore Eye Research Institute, Singapore 169856, Singapore; Ophthalmology and Visual Sciences Academic Clinical Programme, Duke-NUS Medical School, Singapore 169857, Singapore;* orcid.org/0000-0002-5105-0484; Email: andri.kartasasmita.riau@seri.com.sg

Authors

Arun J. Thirunavukarasu − *Tissue Engineering and Cell Therapy Group, Singapore Eye Research Institute, Singapore 169856, Singapore; Oxford University Clinical Academic Graduate School, University of Oxford, Oxford OX3 9DU, United Kingdom*

Fernando Morales-Wong − *Tissue Engineering and Cell Therapy Group, Singapore Eye Research Institute, Singapore 169856, Singapore; Singapore National Eye Centre, Singapore 168751, Singapore; Autonomous University of Nuevo Leon, San Nicolas de los Garza, Nuevo Leon 66455, Mexico*
Nuur Shahinda Humaira binte Halim − *Tissue Engineering and Cell Therapy Group, Singapore Eye Research Institute, Singapore 169856, Singapore*
Evelina Han − *Tissue Engineering and Cell Therapy Group, Singapore Eye Research Institute, Singapore 169856, Singapore*
Siew Kwan Koh − *Ocular Proteomics Group, Singapore Eye Research Institute, Singapore 169856, Singapore*
Lei Zhou − *Department of Applied Biology and Chemical Technology, Hong Kong Polytechnic University, Hung Hom, Hong Kong; Centre for Eye and Vision Research, Shatin, Hong Kong*
Viridiana Kocaba − *Tissue Engineering and Cell Therapy Group, Singapore Eye Research Institute, Singapore 169856, Singapore*
Subramanian Venkatraman − *Department of Materials Science and Engineering, National University of Singapore, Singapore 117575, Singapore; iHealthTech, National University of Singapore, Singapore 117599, Singapore*

Complete contact information is available at: https://pubs.acs.org/10.1021/acsami.4c04077

Notes

The authors declare the following competing financial interest(s): Authors: Subramanian Venkatraman, Jodhbir S Mehta, and Andri K Riau, are co-inventors of a patent (US Patent 11,471,269) that is relevant to the coating technology described in the article.

■ ACKNOWLEDGMENTS

Illustrations of scissors, SEM, and fluorescence microscope were created with BioRender.com (agreement no. BR26PK0EH2). The authors thank Dr. Nyein Chan Lwin, Ms. Hengpei Ang, and Mrs. Mageswari D/O Muthusamy for their assistance with animal experiments. L.Z. thanks the InnoHK initiative and the Hong Kong Special Administrative Region Government. This study was funded by the Duke-NUS Khoo Postdoctoral Award Fund (KPFA/2018/0028) and the SingHealth Foundation Research Grant (SHF/FG661P/2017).

■ REFERENCES

(1) Gain, P.; Jullienne, R.; He, Z.; Aldossary, M.; Acquart, S.; Cognasse, F.; Thuret, G. Global Survey of Corneal Transplantation and Eye Banking. *JAMA Ophthalmol* **2016**, *134* (2), 167−173.
(2) Lagali, N. Corneal Stromal Regeneration: Current Status and Future Therapeutic Potential. *Curr. Eye Res.* **2020**, *45* (3), 278−290.
(3) Matthyssen, S.; Van den Bogerd, B.; Dhubhghaill, S. N.; Koppen, C.; Zakaria, N. Corneal Regeneration: A Review of Stromal Replacements. *Acta Biomater* **2018**, *69*, 31−41.
(4) Thirunavukarasu, A. J.; Han, E.; Nedumaran, A. M.; Kurz, A. C.; Shuman, J.; Yusoff, N. Z. b. M.; Liu, Y.-C.; Foo, V.; Czarny, B.; Riau, A. K.; et al. Electron Beam-Irradiated Donor Cornea for On-Demand Lenticule Implantation to Treat Corneal Diseases and Refractive Error. *Acta Biomater* **2023**, *169*, 334−347.
(5) Isaacson, A.; Swioklo, S.; Connon, C. J. 3D Bioprinting of a Corneal Stroma Equivalent. *Exp. Eye Res.* **2018**, *173*, 188−193.
(6) Price, M. O.; Thompson, R. W., Jr; Price, F. W., Jr Risk Factors for Various Causes of Failure in Initial Corneal Grafts. *Arch Ophthalmol* **2003**, *121* (8), 1087−1092.
(7) Avadhanam, V. S.; Smith, H. E.; Liu, C. Keratoprostheses for Corneal Blindness: A Review of Contemporary Devices. *Clin Ophthalmol* **2015**, *9*, 697−720.
(8) Harissi-Dagher, M.; Dohlman, C. H. The Boston Keratoprosthesis in Severe Ocular Trauma. *Can. J. Ophthalmol* **2008**, *43* (2), 165−169.
(9) Dohlman, C. The Boston Keratoprosthesis-The First 50 Years: Some Reminiscences. *Annu. Rev. Vis Sci.* **2022**, *8*, 1−32.
(10) Basu, S.; Serna-Ojeda, J. C.; Senthil, S.; Pappuru, R. R.; Bagga, B.; Sangwan, V. The Aurolab Keratoprosthesis (KPro) versus the Boston Type I KPro: 5-year Clinical Outcomes in 134 Cases of Bilateral Corneal Blindness. *Am. J. Ophthalmol* **2019**, *205*, 175−183.
(11) Capuani, S.; Malgir, G.; Chua, C. Y. X.; Grattoni, A. Advanced Strategies to Thwart Foreign Body Response to Implantable Devices. *Bioeng. Transl. Med.* **2022**, *7* (3), No. e10300.
(12) Yang, L.; Kong, J.; Qiu, Z.; Shang, T.; Chen, S.; Zhao, R.; Raucci, M. G.; Yang, X.; Wu, Z. Mineralized Collagen-Modified PMMA Cement Enhances Bone Integration and Reduces Fibrous Encapsulation in the Treatment of Lumbar Degenerative Disc Disease. *Regen Biomater* **2020**, *7* (2), 181−193.
(13) Bouhout, S.; Robert, M. C.; Harissi-Dagher, M. Mid-Term Prognosis of Type I Boston Keratoprosthesis Reimplantation. *Br J. Ophthalmol* **2022**, *106* (1), 37−41.
(14) Legeais, J. M.; Renard, G. A Second Generation of Artificial Cornea (Biokpro II). *Biomaterials* **1998**, *19* (16), 1517−1522.
(15) Nascimento, H. M.; Oliveira, L. A.; Höfling-Lima, A. L. Infectious Keratitis in Patients Undergoing Boston Type 1 Keratoprosthesis (Boston KPro) Procedure: Case Series. *Arq Bras Oftalmol* **2011**, *74* (2), 127−129.
(16) Dudenhoefer, E. J.; Nouri, M.; Gipson, I. K.; Baratz, K. H.; Tisdale, A. S.; Dryja, T. P.; Abad, J. C.; Dohlman, C. H. Histopathology of Explanted Collar Button Keratoprostheses: A Clinicopathologic Correlation. *Cornea* **2003**, *22* (5), 424−428.
(17) Eslani, M.; Baradaran-Rafii, A.; Movahedan, A.; Djalilian, A. R. The Ocular Surface Chemical Burns. *J. Ophthalmol.* **2014**, *2014*, No. 196827.
(18) Salvador-Culla, B.; Kolovou, P. E.; Arzeno, L.; Martínez, S.; López, M. A. Boston Keratoprosthesis Type 1 in Chemical Burns. *Cornea* **2016**, *35* (6), 911−916.
(19) Dunne, C. F.; Twomey, B.; Kelly, C.; Simpson, J. C.; Stanton, K. T. Hydroxyapatite and Fluorapatite Coatings on Dental Screws: Effects of Blast Coating Process and Biological Response. *J. Mater. Sci. Mater. Med.* **2015**, *26* (1), 5347−5347.
(20) Geesink, R. G.; de Groot, K.; Klein, C. P. Chemical Implant Fixation Using Hydroxyl-Apatite Coatings. The Development of a Human Total Hip Prosthesis for Chemical Fixation to Bone using Hydroxyl-apatite Coatings on Titanium Substrates. *Clin. Orthop. Relat. Res.* **1987**, *225*, 147−170.
(21) Wang, L.; Jeong, K. J.; Chiang, H. H.; Zurakowski, D.; Behlau, I.; Chodosh, J.; Dohlman, C. H.; Langer, R.; Kohane, D. S. Hydroxyapatite for Keratoprosthesis biointegration. *Invest Ophthalmol Vis Sci.* **2011**, *52* (10), 7392−7399.
(22) Gao, H.; Chen, Y.; Chen, X.; Huang, L.; Yao, H.; Zhu, X.; Tang, M.; Wang, Y.; Li, X.; Xie, L. In Vitro and In Vivo Studies on Bioactive Hydroxyapatite-Coated Magnesium for Glaucoma Drainage Implant. *J. Magnesium Alloys* **2024**. In press. DOI: 10.1016/j.jma.2023.09.033
(23) Shi, X. H.; Wang, S. L.; Zhang, Y. M.; Wang, Y. C.; Yang, Z.; Zhou, X.; Lei, Z. Y.; Fan, D. L. Hydroxyapatite-Coated Sillicone Rubber Enhanced Cell Adhesion and It May Be Through the Interaction of EF1β and γ-Actin. *PLoS One* **2014**, *9* (11), No. e111503.
(24) Rakshit, M.; Gautam, A.; Toh, L. Z.; Lee, Y. S.; Lai, H. Y.; Wong, T. T.; Ng, K. W. Hydroxyapatite Particles Induced Modulation of Collagen Expression and Secretion in Primary Human Dermal Fibroblasts. *Int. J. Nanomedicine* **2020**, *15*, 4943−4956.
(25) Riau, A. K.; Lwin, N. C.; Gelfand, L.; Hu, H.; Liedberg, B.; Chodosh, J.; Venkatraman, S. S.; Mehta, J. S. Surface Modification of Corneal Prosthesis with Nano-Hydroxyapatite to Enhance In Vivo biointegration. *Acta Biomater* **2020**, *107*, 299−312.

(26) Dehghanghadikolaei, A.; Fotovvati, B. Coating Techniques for Functional Enhancement of Metal Implants for Bone Replacement: A Review. *Materials* **2019**, *12* (11), 1795−1795.
(27) Riau, A. K.; Venkatraman, S. S.; Mehta, J. S. Biomimetic vs. Direct Approach to Deposit Hydroxyapatite on the Surface of Low Melting Point Polymers for Tissue Engineering. *Nanomaterials (Basel)* **2020**, *10* (11), 2162.
(28) Riau, A. K.; Venkatraman, S. S.; Dohlman, C. H.; Mehta, J. S. Surface Modifications of the PMMA Optic of a Keratoprosthesis to Improve biointegration. *Cornea* **2017**, *36* (Suppl 1), S15−S25.
(29) Bobzin, K.; Öte, M.; Knoch, M. A.; Heinemann, H. Influence of the Injector Head Geometry on the Particle Injection in Plasma Spraying. *J. Therm Spray Technol.* **2020**, *29* (4), 534−545.
(30) Surmenev, R. A.; Ivanova, A. A.; Epple, M.; Pichugin, V. F.; Surmeneva, M. A. Physical Principles of Radio-Frequency Magnetron Sputter Deposition of Calcium-Phosphate-Based Coating with Tailored Properties. *Surf. Coat. Technol.* **2021**, *413*, No. 127098.
(31) Riau, A. K.; Mondal, D.; Setiawan, M.; Palaniappan, A.; Yam, G. H. F.; Liedberg, B.; Venkatraman, S. S.; Mehta, J. S. Functionalization of the Polymeric Surface with Bioceramic Nanoparticles via a Novel, nonthermal Dip Coating Method. *ACS Appl. Mater. Interfaces* **2016**, *8* (51), 35565−35577.
(32) Du, Y.; Chen, J.; Funderburgh, J. L.; Zhu, X.; Li, L. Functional Reconstruction of Rabbit Corneal Epithelium by Human Limbal Cells Cultured on Amniotic Membrane. *Mol. Vision* **2003**, *9*, 635−643.
(33) Donisi, P. M.; Rama, P.; Fasolo, A.; Ponzin, D. Analysis of Limbal Stem Cell Deficiency by Corneal Impression Cytology. *Cornea* **2003**, *22* (6), 533−538.
(34) Karamichos, D.; Guo, X. Q.; Hutcheon, A. E.; Zieske, J. D. Human Corneal Fibrosis: An In Vitro Model. *Invest Ophthalmol Vis Sci.* **2010**, *51* (3), 1382−1388.
(35) Pei, Y.; Sherry, D. M.; McDermott, A. M. Thy-1 Distinguishes Human Corneal Fibroblasts and Myofibroblasts from Keratocytes. *Exp. Eye Res.* **2004**, *79* (5), 705−712.
(36) Chameettachal, S.; Venuganti, A.; Parekh, Y.; Prasad, D.; Joshi, V. P.; Vashishtha, A.; Basu, S.; Singh, V.; Bokara, K. K.; Pati, F. Human Cornea-Derived Extracellular Matrix Hydrogel for Prevention of Post-Traumatic Corneal Scarring: A Translational Approach. *Acta Biomater* **2023**, *171*, 289−307.
(37) Fenner, B. J.; Liu, Y.-C.; Koh, S. K.; Gao, Y.; Deng, L.; Beuerman, R. W.; Zhou, L.; Theng, J. T. S.; Mehta, J. S. Mediators of Corneal Haze Following Implantation of Presbyopic Corneal Inlays. *Invest Ophthalmol Vis Sci.* **2019**, *60* (4), 868−876.
(38) Patel, S.; Thakar, R. G.; Wong, J.; McLeod, S. D.; Li, S. Control of Cell Adhesion on Poly(methyl methacrylate). *Biomaterials* **2006**, *27* (14), 2890−2897.
(39) Punet, X.; Mauchauffé, R.; Rodríguez-Cabello, J. C.; Alonso, M.; Engel, E.; Mateos-Timoneda, M. A. Biomolecular Functionalization for Enhanced Cell-Material Interactions of Poly(methyl methacrylate) Surfaces. *Regen Biomater* **2015**, *2* (3), 167−175.
(40) Choi, S. M.; Yang, W. K.; Yoo, Y. W.; Lee, W. K. Effect of Surface Modification on the In Vitro Calcium Phosphate Growth on the Surface of Poly(methyl methacrylate) and Bioactivity. *Colloids Surf. B Biointerfaces* **2010**, *76* (1), 326−333.
(41) Riau, A. K.; Mondal, D.; Yam, G. H. F.; Setiawan, M.; Liedberg, B.; Venkatraman, S. S.; Mehta, J. S. Surface Modification of PMMA to Improve Adhesion to Corneal Substitutes in a Synthetic Core-Skirt Keratoprosthesis. *ACS Appl. Mater. Interfaces* **2015**, *7* (39), 21690−21702.
(42) Sharifi, R.; Mahmoudzadeh, S.; Islam, M. M.; Koza, D.; Dohlman, C. H.; Chodosh, J.; Gonzalez-Andrades, M. Covalent Functionalization of PMMA Surface with L-3,4-Dihydroxyphenylalanine (L-DOPA) to Enhance its Biocompatibility and Adhesion to Corneal Tissue. *Adv. Mater. Interfaces* **2020**, *7* (1), 1900767.
(43) Fu, R.; Klinngam, W.; Heur, M.; Edman, M. C.; Hamm-Alvarez, S. F. Tear Proteases and Protease Inhibitors: Potential Biomarkers and Disease Drivers in Ocular Surface Disease. *Eye Contact Lens* **2020**, *46* (Suppl 2), S70−S83.
(44) Stepp, M. A.; Menko, A. S. Immune Responses to Injury and Their Links to Eye Disease. *Transl Res.* **2021**, *236*, 52−71.
(45) Babo, S.; Ferreira, J. L.; Ramos, A. M.; Micheluz, A.; Pamplona, M.; Casimiro, M. H.; Ferreira, L. M.; Melo, M. J. Characterization and Long-Term Stability of Historical PMMA: Impact of Additives and Acrylic Sheet Industrial Production Processes. *Polymers* **2020**, *12* (10), 2198.
(46) Hou, J. H.; Sivaraman, K. R.; de la Cruz, J.; Lin, A. Y.; Cortina, M. S. Histopathological and Immunohistochemical Analysis of Melt-Associated Retroprosthetic Membranes in the Boston Type 1 Keratoprosthesis. *JAMA Ophthal* **2014**, *132* (9), 1133−1136.
(47) Riau, A. K.; Aung, T. T.; Setiawan, M.; Yang, L.; Yam, G. H. F.; Beuerman, R. W.; Venkatraman, S. S.; Mehta, J. S. Surface Immobilization of Nano-Silver on Polymeric Medical Devices to Prevent Bacterial Biofilm Formation. *Pathogens* **2019**, *8* (3), 93.
(48) Hamai, R.; Maeda, H.; Sawai, H.; Shirosaki, Y.; Kasuga, T.; Miyazaki, T. Structural Effects of Phosphate Groups on Apatite Formation in a Copolymer Modified with Ca2+ in a Simulated Body Fluid. *J. Mater. Chem. B* **2018**, *6* (1), 174−182.
(49) Tretinnikov, O. N.; Kato, K.; Ikada, Y. In Vitro Hydroxyapatite Deposition Onto a Film Surface-Grafted with Organophosphate Polymer. *J. Biomed Mater. Res.* **1994**, *28* (11), 1365−1373.
(50) Qu, H.; Wei, M. The Effect of Temperature and Initial pH on Biomimetic Apatite Coating. *J. Biomed Mater. Res. B: Appl. Biomater* **2008**, *87B* (1), 204−212.
(51) Ciolino, J. B.; Belin, M. W.; Todani, A.; Al-Arfaj, K.; Rudnisky, C. J. Retention of the Boston Keratoprosthesis Type 1: Multicenter Study Results. *Ophthalmology* **2013**, *120* (6), 1195−1200.
(52) Prabhasawat, P.; Chotikavanich, S.; Ngowyutagon, P.; Pinitpuwadol, W. Long-term Outcomes of Boston Type I Keratoprosthesis, and Efficacy of Amphotericin B and Povidone-Iodine in Infection Prophylaxis. *Am. J. Ophthalmol* **2021**, *232*, 40−48.
(53) Sun, H.; Hu, Z. L. The Modified Polymethyl methacrylate-Silicone Keratoprosthesis in Rabbit Model. *Int. J. Artif Organs* **2018**, *41* (5), 289−293.
(54) Eaton, J. S.; Miller, P. E.; Bentley, E.; Thomasy, S. M.; Murphy, C. J. The SPOTS System: An Ocular Scoring System Optimized for Use in Modern Preclinical Drug Development and Toxicology. *J. Ocul Pharmacol Ther* **2017**, *33* (10), 718−734.
(55) Chng, C. L.; Seah, L. L.; Yang, M.; Shen, S. Y.; Koh, S. K.; Gao, Y.; Deng, L.; Tong, L.; Beuerman, R. W.; Zhou, L. Tear Proteins Calcium binding protein A4 (S100A4) and Prolactin Induced Protein (PIP) are Potential Biomarkers for Thyroid Eye Disease. *Sci. Rep.* **2018**, *8* (1), 16936.
(56) Kammers, K.; Cole, R. N.; Tiengwe, C.; Ruczinski, I. Detecting Significant Changes in Protein Abundance. *EuPA Open Proteom* **2015**, *7*, 11−19.
(57) Dennis, G., Jr.; Sherman, B. T.; Hosack, D. A.; Yang, J.; Gao, W.; Lane, H. C.; Lempicki, R. A. DAVID: Database for Annotation, Visualization, and Integrated Discovery. *Genome Biol.* **2003**, *4* (5), P3.

https://doi.org/10.1021/acsami.4c04077
ACS Appl. Mater. Interfaces 2024, 16, 25892−25908